



Analysis of pigments and mortars from the wall paintings of the Roman archaeological site of *Las Dunas* (San Pedro de Alcántara, Malaga S Spain)

M. Urosevic^a, D. Jiménez-Desmond^b, A. Arizzi^{a,*}, J.S. Pozo-Antonio^b, C. Moreno Prieto^c, M. Vila Oblitas^c

^a Dpt. of Mineralogy and Petrology, Faculty of Science, University of Granada, 18071 Granada, Spain

^b CINTECX, GESSMin group. Dpt. of Natural Resources and Environmental Engineering, School of Mining and Energy Engineering, University of Vigo, 36310 Vigo, Spain

^c Menia. Restauración & Patrimonio, C/Gladiolos, 29651 Mijas Costa, Malaga, Spain

ARTICLE INFO

Keywords:

Roman wall painting
Magnesian (dolomitic) lime
Hydraulic mortars
Marine environment
Local geology

ABSTRACT

This study aims to describe the composition, texture, and arrangement of mortars and pictorial layers from a newly excavated Roman archaeological site in the province of Baetica, southern Spain. Representative fragments with well-preserved pictorial layers were analyzed using optical imaging, spectrophotometry, Scanning Electron Microscopy with Energy-Dispersive Spectroscopy (SEM-EDS) mapping, and X-ray diffraction. The results reveal similarities to other well-studied Roman archaeological sites, particularly in the use of mixtures of natural (hematite, goethite, aragonite, phyllosilicates, and quartz) and synthetic minerals (cuprorivaite) used in classical Roman pigments. However, the mortar from the investigated site shows a distinctive use of ferromagnesian silicates (olivine and pyroxenes from local ultramafic rocks) as aggregate material, making this site unique among all Roman provinces. Additionally, the common occurrence of Mg in the binder of the mortars under the form of brucite, hydromagnesite and magnesium silicate hydrates, indicates the use of a magnesian (dolomitic) lime that, according to the chemical analyses, was obtained by adding up to 15 wt% of powdered dolomitic marbles from nearby Roman quarries to the limestone. We speculate that this addition might be intended to improve the workability and mechanical resistances of the mortar in combination with the abundant ferromagnesian silicates used as aggregates, some of them showing chemically reactive rims in contact with the binder. In conclusion, this study provides further evidence of the advanced knowledge and skills achieved by Roman craftsmen who were able to adapt traditional recipes to suit local resources, obtaining materials of excellent quality and durability.

1. Introduction

The discovery of Vesuvian wall paintings in Pompeii, Herculaneum, and Stabiae in the 18th century sparked a keen interest in studying the techniques and pigments used by the ancient Romans to create wall paintings (Aliatis et al., 2011; Bergamonti et al., 2022; Cuní, 2016). The well-preserved condition of these paintings offered an unparalleled opportunity for research. However, until the end of the 20th century, research on Roman wall paintings in other Roman provinces such as those in Spain was characterized by limited international publications (Abad Casal, 1982; Cánovas Ubera, 1999; Cerrato Moreno, 2021; Cortea et al., 2021; Lewit, 2008), and only recently has it gained significant interest (Giménez Rodríguez, 2021). Despite some recent contributions (Alcántara et al., 2022; Cerrato et al., 2021; Cuní, 2016; Durán et al.,

2011; Piovesan et al., 2011; Salvadori and Sbroli, 2021; Tuñón et al., 2020), there is still a lack of studies considering the vast archaeological heritage, particularly in southern Spain, such as the Roman province of Baetica (Belén et al., 1998; Fig. 1a).

Although many classical authors have described the methodology followed in rendering wall paintings, including Vitruvius, Cato, Pliny, Columella, Palladius, and Faventinus (DeLaine, 2021; Lancaster, 2021; Salvadori and Sbroli, 2021; Calabria Salvador and Zalbidea Muñoz, 2019), classical sources on the specific Spanish case are practically absent (Abad Casal, 1982; Benlloch, 2006). Therefore, identifying the pigments and paint recipes remains one of the most critical unanswered questions (Piovesan et al., 2011). Furthermore, throughout history, the mixing of different pigments to create other colours has been a constant practice, as evidenced by Pompeian paintings, such as the combination

* Corresponding author.

E-mail address: arizzina@ugr.es (A. Arizzi).

<https://doi.org/10.1016/j.jasrep.2023.104280>

Received 29 June 2023; Received in revised form 20 October 2023; Accepted 23 October 2023

Available online 6 November 2023

2352-409X/© 2023 The Author(s). Published by Elsevier Ltd. This is an open access article under the CC BY-NC license (<http://creativecommons.org/licenses/by-nc/4.0/>).

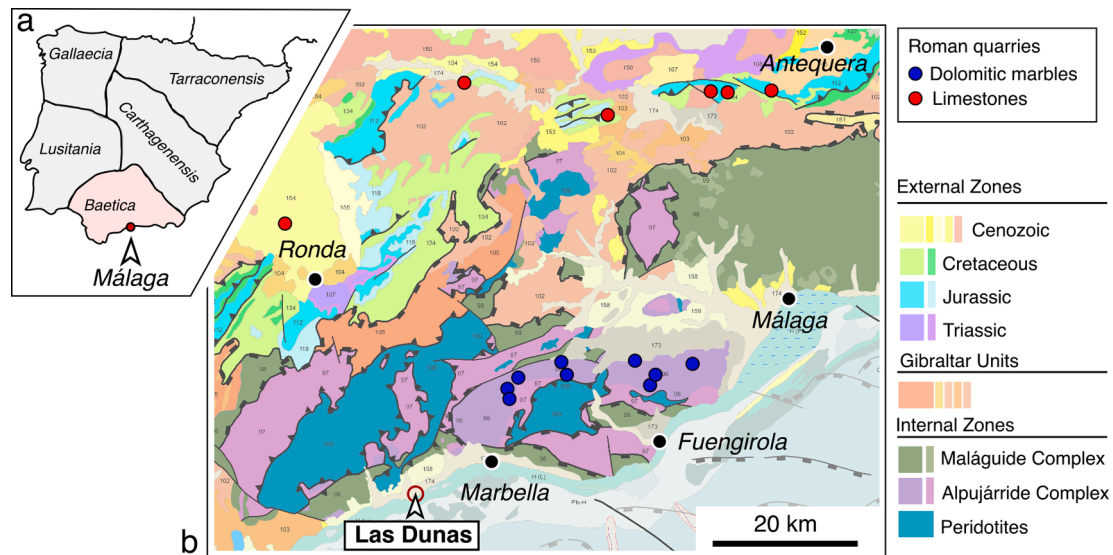


Fig. 1. A) Diocletian's provincial division of Hispania in the 3rd century BCE (Iberia), Malaga (Malaca) in the Baetica province is highlighted. b) Geological map of Western Malaga (IGME and LNEG, 2015) and location of the Las Dunas Roman site. Identified ancient Roman quarries for marble (Lapuente et al., 2022) and limestones (Ontiveros-Ortega et al., 2019) are indicated by blue and red dots respectively. (For interpretation of the references to colour in this figure legend, the reader is referred to the web version of this article.)

of malachite with Egyptian blue or yellow ochres (Aliatis et al., 2009, 2011; Siddall, 2018).

This study aims to contribute to the understanding of the composition, texture, and arrangement of mortars and pigments in the wall paintings of a recently exposed Roman archaeological site in the province of Baetica, southern Spain (Fig. 1a), using modern analytical techniques to identify similarities and differences in the raw materials used. This investigation will shed light on the technical knowledge of Roman craftsmen in adapting traditional recipes to local natural resources, as well as the geological context and availability of raw materials that may have influenced their techniques. Moreover, the present study will add new insights into the artistic and cultural practices of ancient civilizations to the limited body of knowledge on Roman wall paintings in the Baetica Roman province.

2. Geological context

The province of Baetica in the Roman Empire encompassed a vast territory comprising a notable variety of geological units and lithologies. The geological features of the materials exposed in this region rendered the location and extraction of calcareous stone materials relatively not particularly difficult. As a consequence, the employment of *marmora* (comprising marble, limestone, and travertine) became prevalent in Baetica during the early imperial period (Beltrán Fortes et al., 2011).

The geological setting of the Western Malaga archaeological site, situated in the Alpine Betic chain, is exceptionally intricate (as illustrated in Fig. 1b). Considering the importance of the geological context in identifying the origin of the utilized raw materials, a concise summary is provided herein. The Alpine orogeny led to the collision of allochthonous terranes (Internal Units) with the Meso-Cenozoic paleomargins (External Units) to the South of the Iberian plate (e.g. Jabaloy Sánchez et al., 2019 and references therein). Both Units are represented in

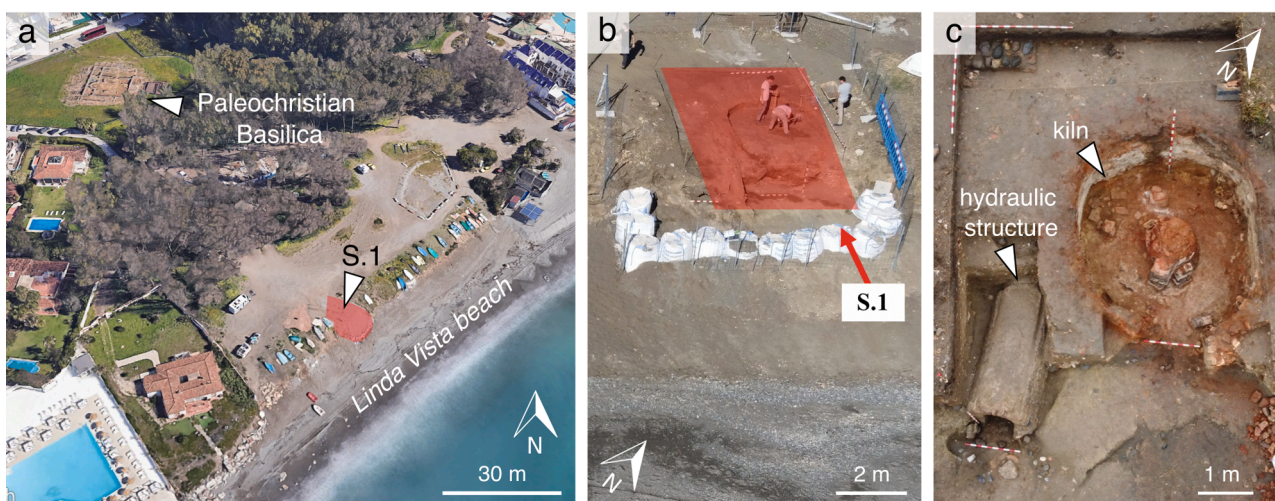


Fig. 2. a) Aerial view of Linda Vista beach (Google Earth). b) Marked in red is the location of Survey 1 (S.1), one of the five surveys carried out during the archaeological activity of 2021; c) aerial view of survey 1 (S.1) where a kiln and a hydraulic structure is well preserved. (For interpretation of the references to colour in this figure legend, the reader is referred to the web version of this article.)

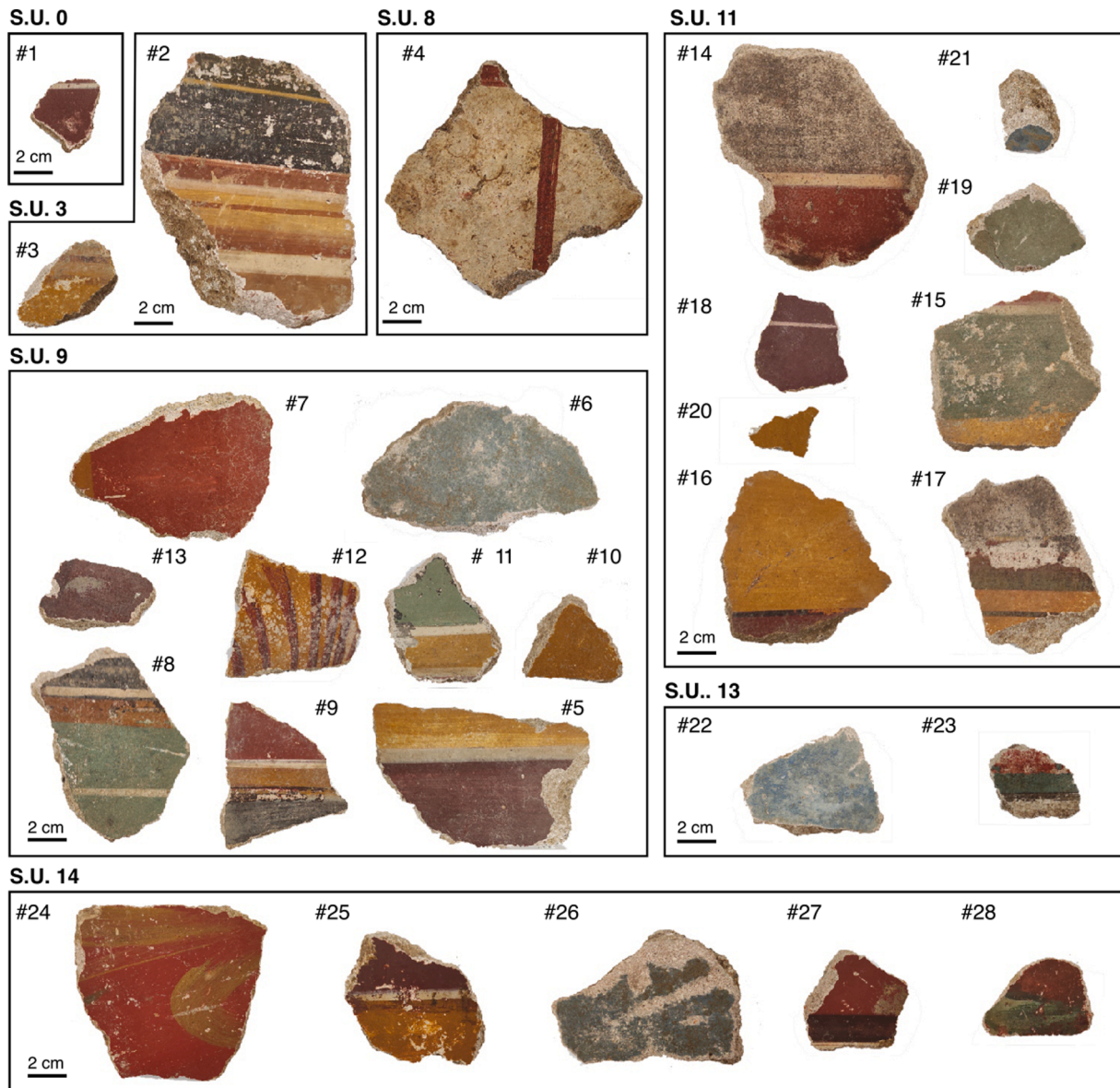


Fig. 3. Macroscopic view of investigated mural fragments grouped by archaeological location site. All images at the same scale.

Western Malaga and are separated by the Gibraltar Units marking the suture of the orogenic belt (Fig. 1b). Notably, Western Malaga encompasses both the Internal Units, including several marble sequences that were exploited since the Roman era (indicated by blue dots in Fig. 1b) and a unique occurrence of a large orogenic peridotite (Ronda Peridotite), located North of the investigated archeological site. The Ronda Peridotite comprises lherzolite and harzburgite (ultramafic rocks containing more than 40 vol% of olivine) with subordinate dunite and pyroxenite layers. In addition, various Roman quarries exploiting limestone are known from the External Units in Western Malaga (as represented by red dots in Fig. 1b).

3. Archaeological context

The archaeological site of *Las Dunas* is situated in the ancient Roman province of Baetica, which currently covers a large portion of Andalusia and the southern region of Extremadura (Alayón et al., 2021, cf. Fig. 1a). The province was established during the Augustan Age (1st century CE) and consisted of colonies and cities such as *Hispalis* (Seville), *Corduba* (Córdoba), and *Malaca* (Malaga), among others. Archaeological

evidence indicates the existence of villas, centers for the production of amphorae, and grain, wool, and wine centers, although their economic importance primarily depended on the trade of olive oil and salted fish (*garum*) (Bagnall et al., 2013; Fear, 1996; Velasco, 2018).

On the coasts of the Mediterranean Sea, we find a not well-recognised Roman archaeological site known as *Las Dunas* (in *Linda Vista Beach*, San Pedro de Alcántara, Marbella, Malaga) (Fig. 2), settlement of a large production centre of building materials during the 4th and 5th centuries AD (Moreno Prieto and Vila Oblitas, 2022). The archaeological site is an important settlement known to historiography since the beginning of the 20th century due to the discovery of an early Paleochristian Basilica and an extensive necropolis, located 100 m to the northwest of the site of *Las Dunas* (see Fig. 2a). Such was the importance of the findings that the site soon acquired the category of heritage of cultural interest, the highest legal status for the protection of Spanish historical heritage (Moreno Prieto and Vila Oblitas, 2022). Although this site is still buried underground, thorough archaeological studies have been carried out (Moreno Prieto and Vila Oblitas, 2022; Pérez de Barradas, 1930; Pérez de Barradas, 1932; Pérez de Barradas, 1934; Puertas and Posacs, 1989; Puerto et al., 2017; Requena, 2021; Villaseca and

Table 1
Representative samples and techniques used in this study.

Sample ID	Stratigraphic Unit (S.U.)	Inventory number	Red	Yellow	Green	Blue	Black	White	Total Thickness (mm)	Intonaco (mm)	μXRD	OM	ESEM
1	0	25	○	○	○	○	○	●	11.9	5.5	●		
2	3	114	○	○	○	○	○	●	42.6	12.6		●	
3	3	114	●	○	○	○	○	○	16.2	n.o.			
4	8	183	○	○	○	○	○	○	19.8	n.o.		●	
5	9	49	○	●	○	○	○	●	24.8	7.1			
6	9	49	○	○	○	○	○	○	31.3	5.0			
7	9	49	○	○	○	○	○	○	31.1	n.o.	●		
8	9	49	●	○	○	○	●	●	33.1	10.5		●	
9	9	49	○	●	○	○	○	●	22.1	6.5	●		
10	9	49	○	○	○	○	○	○	19.0	7.0			
11	9	49	○	○	○	○	○	○	24.2	10.0			
12	9	49	○	○	○	○	○	○	21.5	6.3			
13	9	49	○	○	○	○	○	○	18.0	n.o.	● *	●	● **
14	11	71	○	○	○	○	○	●	42.7	6.7		●	
15	11	71	●	●	○	○	○	●	26.9	5.8	●	●	
16	11	71	○	○	○	○	○	○	24.9	6.5	●	●	
17	11	71	○	○	○	○	○	○	18.6	4.9	●	●	
18	11	71	○	○	○	○	○	●	13.8	5.2	●	●	●
19	11	71	○	○	○	○	○	○	30.0	11.6	●	●	●
20	11	71	○	○	○	○	○	○	13.7	5.9	●	●	●
21	11	71	○	○	○	○	○	○	31.1	6.8	●	●	●
22	13	127	○	○	○	○	○	○	20.6	8.1		●	
23	13	127	●	○	○	○	○	○	30.4	8.0			
24	14	202	○	●	○	○	○	○	31.0	5.6	●		
25	14	202	○	○	○	○	○	●	25.7	n.o.			
26	14	202	○	○	○	○	○	○	32.8	6.4			
27	14	202	○	○	○	○	○	○	20.4	5.7			
28	14	202	○	○	○	○	○	○	20.1	6.3			

○ main colour ● colour present ○ colour not present. n.o. not observed with naked eyes. *: also XRD was performed on this sample; **: also SEM EDS was performed on this sample

Garrido, 1991), showing the importance of the site. The geophysical study carried out between 10 and 25 m away from the site of *Las Dunas* (Puerto et al., 2017) detected an intense network of structures dated between the early and late imperial period, undoubtedly related to the remains found in 2021.

Following the exposure of a series of archaeological structures and materials during the 2021 storm, the corresponding government institutions authorized an emergency intervention that was carried out by Moreno Prieto and Vila Oblitas (2022) and their team, aimed at the archaeological characterisation and stratigraphic documentation of the site, as well as the consolidation and protection of the discovered structures. Five surveys were opened for this purpose. The intervention yielded the documentation of up to four ovens and a very well-preserved hydraulic drainage structure. The primary focus of the research was survey one (S.1) (Fig. 2a and b), where the combustion chamber of a large ceramic container production oven was identified (Fig. 2c). The excavation of this area yielded important archaeological remains, including polychrome stuccoes, several bronze artifacts, tesserae, and various construction elements, that can be attributed to a wide range of chronologies between the first and fifth centuries AD. These findings suggest a domestic space such as a *villa a mare* or *thermae* and demonstrate the significant potential and value of the archaeological site of *Las Dunas*, covering a chronology that extends from the high imperial period to at least the sixth century AD (Moreno Prieto and Vila Oblitas, 2022).

4. Materials and methods

4.1. Sampling protocol

The investigated archaeological site (“*Las Dunas*”) is located in San Pedro de Alcántara (Marbella, W of Malaga, S Spain, Fig. 2). From more than one hundred fragments found, a set of 28 samples were selected according to colour palette, aiming to characterize all the different colours present among all fragments (red, yellow, green, blue, black and white, see Fig. 3). Additionally, as the fragments were found in a coastal

environment, and were therefore highly deteriorated by saline efflorescence (e.g., sodium chloride), their conservation state was also considered, selecting those better preserved so as to enable a proper characterization of the materials. All studied fragments (Fig. 3) correspond to wall paintings found as sedimentary fillings in S.1 related to the possible abandonment of the *balnae* of a villa a mare or *thermae*, either of them located in the immediate vicinity. The kiln found in S.1 rests on a singular hydraulic structure (Fig. 2c), interpreted as a large water drain, probably the sewer of this villa or *thermae*. The stratigraphic unit (S.U., Table 1) is related to the level at which each fragment of wall painting has been found. Therefore, S.U. 0 corresponds to the superficial level without excavation, while S.U. 14 is at a greater depth.

4.2. Analytical techniques

Macroscopic observations of the mural fragments’ surfaces were imaged with a binocular stereo microscope (Leica VDM 2000) powered with the Leica Application Suite V.3.8.0 for image acquisition. Textural characterization at this scale includes the identification of the different colour layers, weathering products on the surface (notably marine salt precipitates) and macroscopic porosity.

The chromatic parameters of the different coloured bands in the pictorial layer of the mural fragments were measured with a Minolta CM-700d spectrophotometer with a pulsed xenon lamp (UV cut filter) and an integrating sphere 40 mm in diameter, in specular component excluded (SCE) mode, using a spot diameter of 5 mm, illuminant D65, and 10° observer angle. The colorimetric measurements were performed only on bands thicker than 5 mm, consisting of two consecutive measurements on each point. The CIE 1976 chromatic scale was used to measure the chromatic parameters L^* , a^* and b^* (Wyszecki and Stiles, 1982). L^* is the lightness which varies from black with a value of 0 to white with a value of 100; a^* varies from + a^* (red) to - a^* (green) and b^* ranges from + b^* (yellow) to - b^* (blue).

The mineralogical composition of pigment layers was determined by micro-X-ray diffraction. No sample preparation was required as the

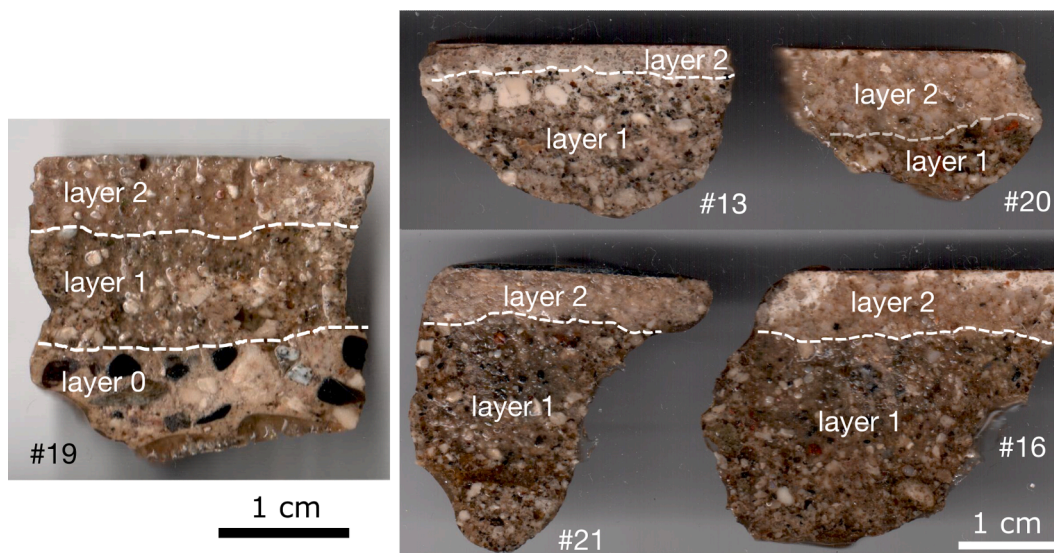


Fig. 4. Representative examples of sections perpendicular to the surface of the mural sample fragments where the top layer is the pictorial layer above the mortar. Two layers (or three in the case of sample #19) below the pictorial layer can be distinguished.

analysis was carried out directly on the surfaces. The X-ray diffraction was acquired with a Bruker D8 Discover using a Pilatus3R 100 K-A detector. Analysis conditions were: radiation Cu K α ($\lambda = 1.5406 \text{ \AA}$), 50 kV voltage and 1 mA current intensity. The angular range measured was from 5° to 86° 2θ and the goniometer speed of 30 s/step. Mineral identification was performed using X'pert HighScore 4.9 (Malvern Panalytical) software.

Mineralogical and textural characteristics of mural fragments including the mortar and the pictorial layers were examined under binocular polarized optical microscope using a CarlZeiss Jenapol-U equipped with a digital camera (Nikon D7000). Observations were made in transmission and reflection mode using both plane-polarized and cross-polarized light to identify the binder and the aggregates of the mortars and the pigments in the pictorial layers. Polished thin sections perpendicular to the surface (stratigraphic sections) were carefully prepared and partly stained with red alizarin to be able to distinguish between calcite and dolomite (calcite is stained to red while dolomite remains unstained).

The chemical composition of mortars (aggregate and binder) was determined using a Quanta400 environmental scanning microscopy (ESEM) and an AURIGA Focused Ion Bombardment CrossBeam Workstation, incorporated into a High-Resolution Field Emission Scanning Electron Microscope (FIB-FESEM) from Carl Zeiss SMT on uncoated polished thin sections, that were previously studied by optical microscopy. Both electron microscopes were equipped with an EDS micro-analyzer. Operation conditions were 20 kV and a working distance of approximately 10 mm. The qualitative elemental mapping was carried out using a standardless P-ZAF correction method, whilst the quantitative EDS point analysis was carried out using a Co standard.

To confirm the nature of the mortar's binder, one of the samples studied under SEM-EDS was crushed by hand and then sieved to mechanically separate the aggregate from the binder. Two sieve fractions (0.125 and 0.050 mm) were analysed by means of X-Ray diffraction (XRD), with an X'Pert Pro Diffractometer (disordered crystalline powder method). Experimental conditions were as follows: 45 kV voltage; 40 mA current; CuK α radiation ($\lambda = 1.5405 \text{ \AA}$); $4\text{--}70^\circ$ 2θ explored area; 0.01° 2θ /s goniometer speed; continuous sample rotation system. Data treatment was performed using the X'pert HighScore 4.9 (Malvern Panalytical) software. Not all samples were analysed by XRD because of the archaeological origin of the mortar pieces.

5. Results

5.1. Macroscopic observations

The selected fragments for this study have irregular shapes and range in size from ca. 3 to 10 cm (Fig. 3) and thickness from 1.2 to 4 cm (see Table 1 for details). At the macroscopic scale and below the painted surface it can be observed the occurrence of a distinctive light-coloured and homogenous layer referred to in the following as layer 2 (or "intonaco" layer, see Fig. 4) in nearly all fragments investigated in this study. Layer 2 is characterized macroscopically by the lack of "cocciopesto" (broken bricks) and dark mineral grains. The thickness of layer 2 ranges from 5 to 12 mm (with an average value of 7 mm, see Table 1 and Fig. 4). Below layer 2, layer 1 is characterized by a high abundance of red coloured "cocciopesto", rounded large white lime lumps and dark mineral grain fragments.

Among all investigated samples, only one (sample #19) showed a distinctive layer below layer 1 and 2 thus resulting in a stratigraphy of three layers (see Fig. 4). The most inner layer in sample #19 (layer 0) is characterized by much larger grain size ($>5 \text{ mm}$) of aggregates that also differ from the other layers in terms of shape (very rounded) and nature of the aggregates. Macroscopically this layer is characterized by the dark/black colour of the coarse fragments constituting the aggregate (Fig. 4).

Most fragment surfaces have several coloured straight layers (Figs. 3 and 5), except for one sample (#12) where alternating layers are slightly curved (Fig. 3). Monochromatic fragments represent only 32 % of the total whereas fragments with more than two different colours represent 43 % of the sampling. Most layers have a width of ca. 1 cm, but thin layers are also common and have a width of less than 3 mm (Figs. 3 and 5). Thin layers are commonly formed by white/light colours and occasionally black or dark red. Most fragments are well preserved and in some rare cases (#24, Fig. 3) yellowish brushstrokes can still be observed on top of the red basic substrate. For blue and green coloured fragments, homogeneously distributed blue crystals (identified as cuprorivaite, see later) can be easily observed with the aid of the binocular. Some straight marks parallel to the layers can also be observed under the binocular suggesting the use of hard polishing tools.

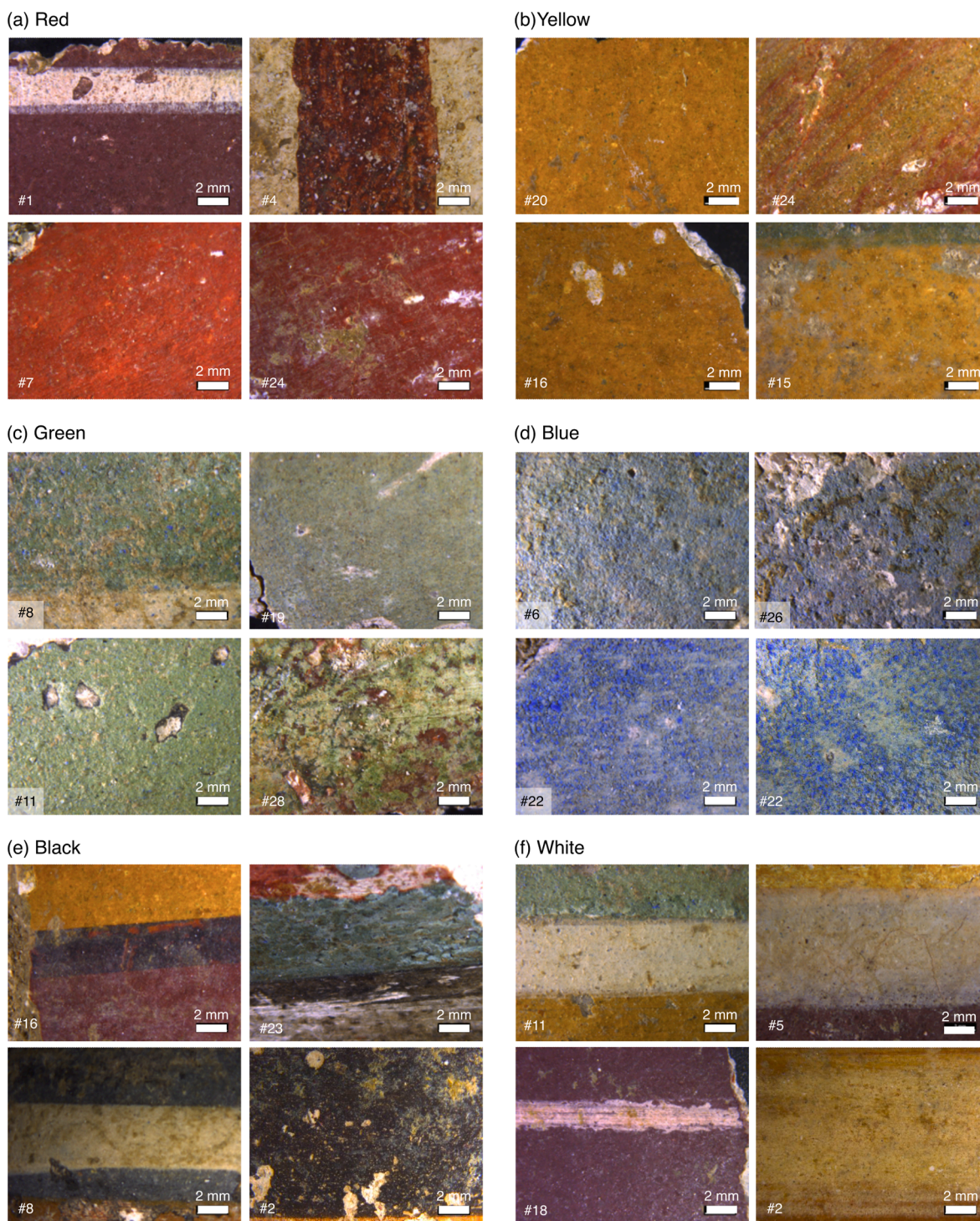


Fig. 5. Digital Video Microscope (DVM) images of representative surface samples for the six groups classified according to the main colour (a) red, (b) yellow, (c) green, (d) blue, (e) black and (f) white. All images are at the same scale (c.f. Table 1). (For interpretation of the references to colour in this figure legend, the reader is referred to the web version of this article.)

5.2. Spectrophotometry

The different measurements were grouped in terms of the main apparent colour (red, yellow, green, blue, black, and white). The first set of colorimetric measurements was conducted on samples as they were collected (referred to as “untreated” in the following). Untreated samples from different groups are well separated in the colour space formed by the a^* (D65) (red-green axis) and b^* (D65) (yellow-blue axis) parameters (Fig. 6a). Moreover, there is a relatively strong correlation

between the a^* and b^* parameters among the colour groups, although untreated samples from the black and red group show more dispersion (Fig. 6a). It was early noticed that untreated samples contained abundant salt crystals (see section 5.4.2) on the surface due to their preservation conditions in a marine environment. Heterogenous distribution of such salts could significantly modify their colour properties, and therefore, all surfaces from the same samples were cleaned using cellulose pulp and deionized water *empacos*, in successive desalination washings, and referred to in the following as “treated” samples. For a

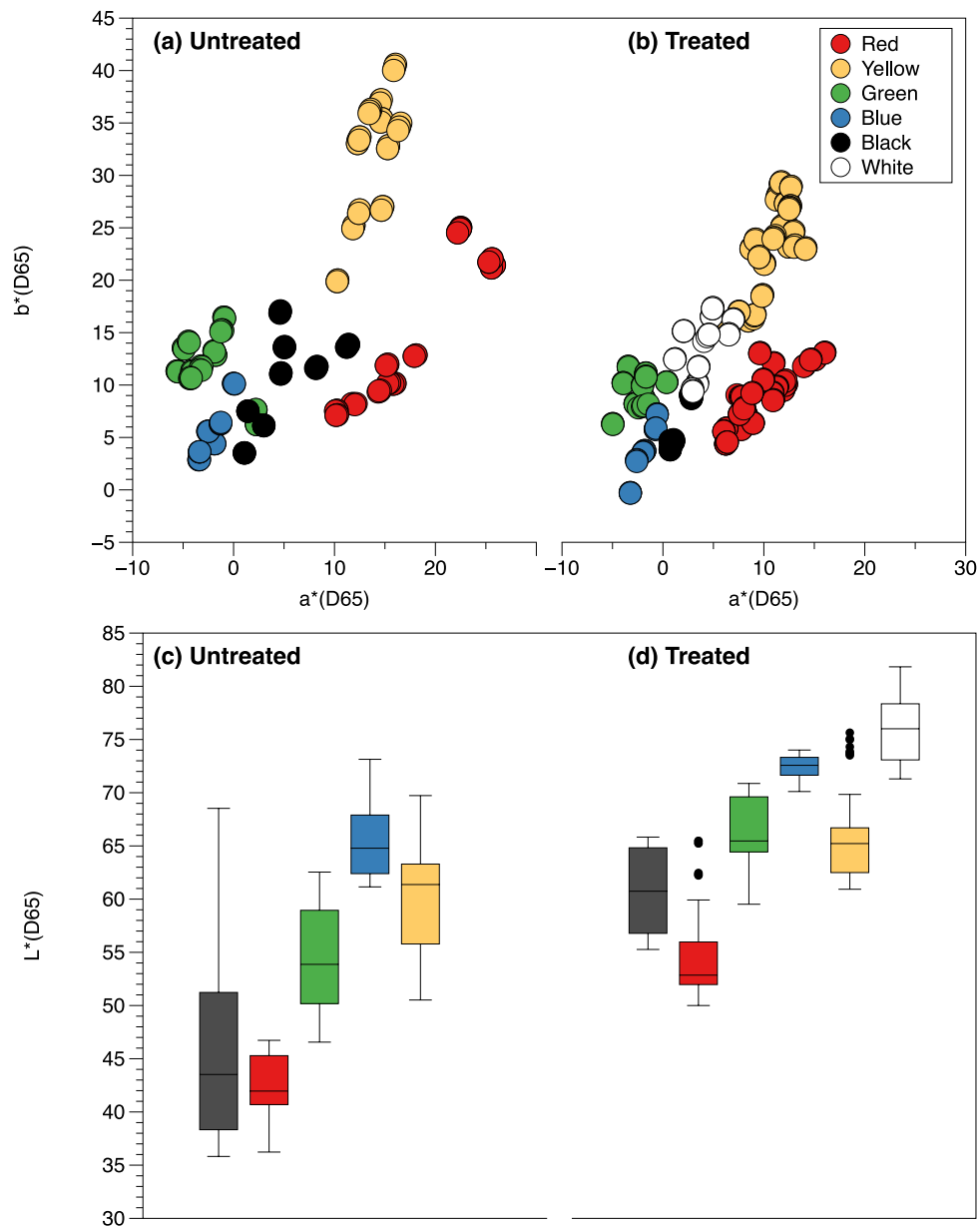


Fig. 6. Quantitative measurements of the colour surfaces by means of spectrophotometry. Upper panel shows the variations in the absolute chromatic values of a^* (D65) (red-green axis) and b^* (D65) (yellow-blue axis) parameters for the six colour groups before (a) and after (b) treatment to dissolve salts on the surface. The lower panel show the range of variation in lightness (L^*) (box-and-whisker plots) for the six identified colour groups before (a) and after (b) the treatment. The horizontal line in the boxes are the median values and the upper and lower box values are the upper and lower quartile, upper and lower extreme values are also represented. Black dots are outliers. (For interpretation of the references to colour in this figure legend, the reader is referred to the web version of this article.)

more straightforward comparison, measurements were conducted on the very same spot after surface treatment. White colour for untreated samples could not be measured due to the profuse occurrence of the salts on the surfaces that are more difficult to avoid for the narrow white layers.

After treatment, different groups show less dispersion and a narrower distribution in terms of a^* and b^* . This effect is more pronounced for the black and red colour layers (Fig. 6b). Although a linear correlation among a^* and b^* still holds for treated samples, only for blue, red, and yellow this correlation is clear. White colour and especially green and black colours are rather homogenous in terms of the a^* and b^* parameters for the treated samples.

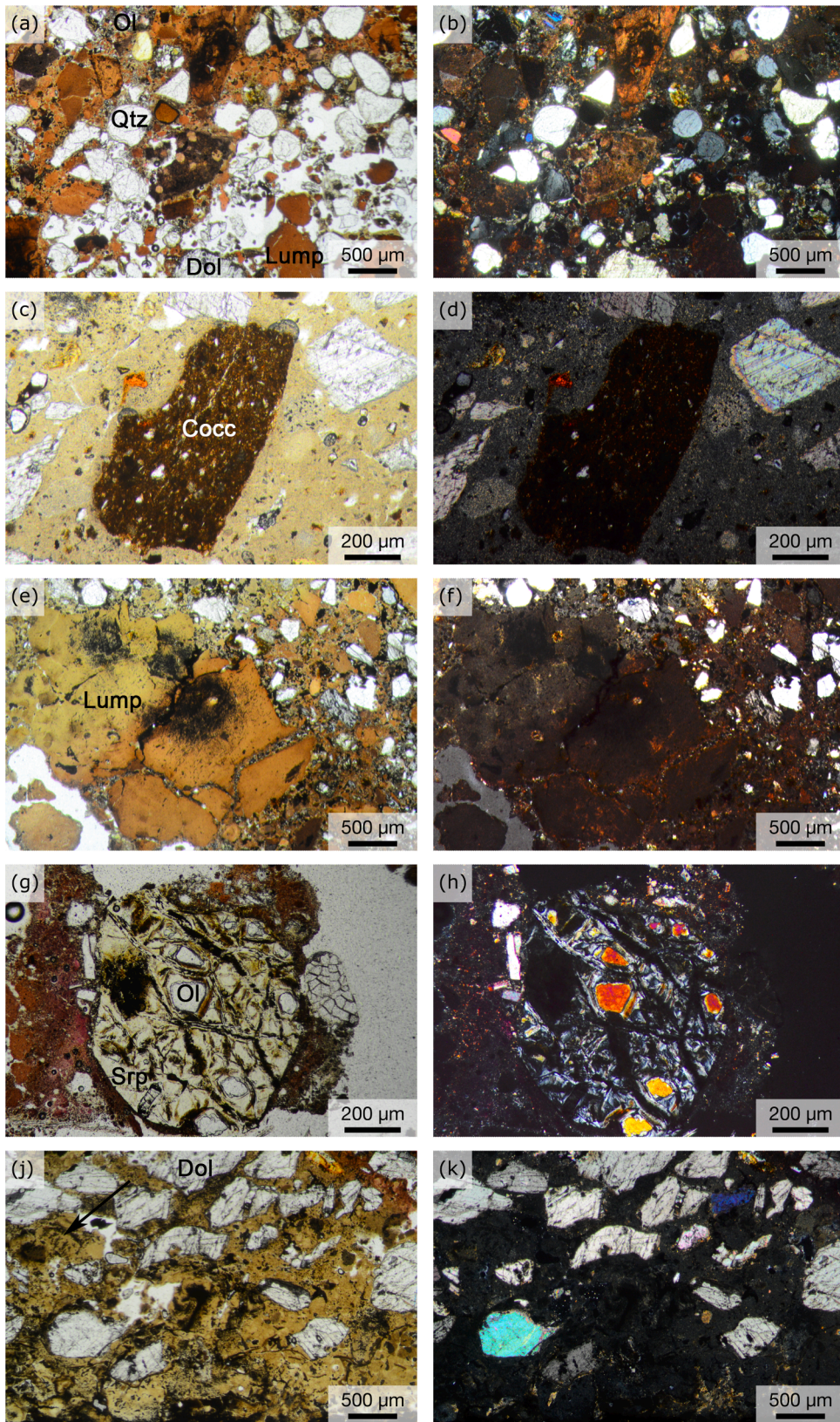
The effect of surface treatment is also evident for the lightness, L^* (D65), where untreated samples show a large dispersion of this

parameter, notably in the case of the black colour (Fig. 6c). After the surface treatment, the groups sorted in increasing values of L^* are red, black, yellow, green, blue, and white (Fig. 6d). Because of the narrower L^* distribution for the treated samples, it is possible to detect the occurrence of some outliers at higher values (black dots in Fig. 6d).

5.3. Petrographic, chemical and mineralogical characterization of the mortar layers

5.3.1. Layer 0

As commented above (see section 5.1), only sample #19 showed a third inner layer that was probably lost in the other samples. The most distinctive feature of layer 0 is that aggregates consist of rock fragments (fine-grained mylonitic calcitic marble, mylonitic gneiss, deformed



(caption on next page)

Fig. 7. Representative optical microscope images of the mortars. Plane polarized (a) and crossed polarized (b) images of sample #21 showing the compositional and textural complexity of layer 1 dominated by aggregates of different nature (mostly rounded quartz grains (*Qtz*), angular dolomite grains (*Dol*), serpentinized olivine (*Ol*) and pyroxenes), abundant rounded lime lumps (alizarin red stained) in a mainly calcitic binder (alizarin red stained). Plane polarized (c) and crossed polarized (d) images from sample #18 (non-stained thin section) showing an irregular “cocciopesto” (broken bricks (*Cocc*)) located in layer 2 with abundant large angular dolomite grains. The fine-grained binder is homogenous. Plane polarized (e) and crossed polarized (f) images from sample #16 of a large calcitic lump (note the red colour in the stained part of the thin section on the lower right) showing desiccation cracks and dark impurities concentrated in the center. Plane polarized (g) and crossed polarized (h) images from sample #22 of an almost completely serpentinized olivine (*Ol*) grain with high interference colours (see Fig. 5h) resulting in a typical serpentinized (*Srp*) mesh texture from layer 1. Plane polarized (j) and crossed polarized (k) representative images of layer 2 of sample #21 where aggregates are almost exclusively formed by coarse (>500 μm) angular dolomite (*Dol*) grains dispersed in the binder. The arrow indicates the dendritic morphology of some brownish patches in the binder and the lime lumps. (For interpretation of the references to colour in this figure legend, the reader is referred to the web version of this article.)

quartzite and serpentinized peridotite) rather than individual mineral grains.

5.3.2. Layer 1

By optical microscopy, the inner layer of mortars (layer 1) appears to be compositionally and texturally complex. The aggregates are heterogeneous, mainly including rounded spherical mono-crystalline quartz grains (Fig. 7a and b) and occasionally mono-crystalline dolomite. Porosity in this layer is abundant and highly irregular (Table 2). It is noticeable the striking occurrence of fine-grained (<200 μm) ferromagnesian silicates such as pyroxenes, olivine and amphiboles (identified by their middle second- to third-order interference colours and further confirmed with EDS analyses, see below) (Fig. 7a and b). Rare occurrences of small (<100 μm) polycrystalline mafic rocks consisting of pyroxene and calcic plagioclase (gabbro) have been also noticed (and confirmed with EDS analyses). Layer 1 further contains abundant fragments of bricks (referred to in the literature as “cocciopesto”, Fig. 7c and d), that can be easily distinguished by their reddish to very dark colour at naked eyes and in (alizerin unstained) plane-polarized images. “Cocciopesto” fragments contain small angular fragments of minerals. Sub-rounded to rounded lime lumps are also very frequent (Fig. 7e and f), some of them showing shrinkage fissures. Partially to completely serpentinized olivine grains are not uncommon (Fig. 7g and h).

5.3.3. Layer 2

Optical microscopic observations confirm that layer 2 is clearly distinguishable from a textural point of view due to (i) its higher binder/aggregate ratio, (ii) lower porosity and (iii) a higher mineralogical purity of the aggregate compared to layer 1 (Fig. 7j and k). The aggregate in layer 2 is mostly composed of relatively coarse-grained (up to 1 mm in length) mono-crystalline angular fragments of dolomite (most likely from a coarse-grained dolomitic marble, Fig. 7j and k). Dolomite grains occasionally show polysynthetic twinning. Although monocrystalline dolomite grains are the most common aggregate, a rare occurrence of a large (4 mm in length) polycrystalline calcitic marble (alizerin stained) has been also observed (this later showing mylonitic texture with abundant metamorphic recrystallization). Minor shrinkage cracks in the binder can be observed. Rare lime lumps, “cocciopesto”, quartz and ferromagnesian silicates can be occasionally observed in layer 2 but are far less frequent than in layer 1.

Under optical microscopy, the fine-grained and homogenous binder of the mortars is compositionally dominated by calcite (alizerin stained, Fig. 7j), even though coarser, and more heterogenous areas that only partially stained with red alizerin were observed. Diffused brownish patches are also visible in the lime lumps and the binder of layer 1 and 2 (Fig. 7e and 7j), some of them even showing a dendritic structure (indicated by an arrow in Fig. 7j), similar to those observed in ancient magnesian lime mortars (Diekamp et al., 2009).

5.3.4. Chemical and mineralogical analysis of the mortars

To confirm the nature of the mortars, sample #13 was analysed by means of EDS (Fig. 8). The matrix of “cocciopesto” fragments is very fine-grained and chemically complex (Mg, Al, Si, K, and minor Ca). The sporadic occurrence of Cl in most EDS analyses of the binder suggests

that the precipitation of marine salts was not restricted to the surface but also penetrated through the porous network of the mortar. Sulphur (S) was detected on only one occasion (layer 2 in sample 20), likely as a secondary component in the binder.

EDS analyses of the mortar aggregates confirmed the occurrence of quartz (Fig. 8 and SM1, spectra 5, 6 and 11), K-feldspar (and/or mica muscovite), serpentine minerals, other ferromagnesian silicates such as olivine and pyroxenes (with distinctive presence of Ti, Fig. 8 and SM1, spectra 1, 2, 3, 4 and 12, and occasionally Cr), amphiboles, gneiss fragments (formed by biotite and K-feldspars), micro-gabbros (formed by plagioclase and pyroxenes, Fig. 8 and SM1, spectra 3, 12 and 13) and iron-rich oxides (likely magnetite and/or hematite).

EDS analyses in both the binder and the lime lumps revealed the presence of some minor amounts of magnesium and silicon (Fig. 8 spectrum 7 and SM1, spectra 8, 9, 10 and 14).

To understand the origin of these elements in the binder, XRD analysis was carried out on the two finest sieved fractions of sample #13 (0.125 and 0.005 mm), after separation from the coarser aggregate grains. As shown in Fig. 9, calcite is the major phase identified in the binder, followed by small amounts of quartz (whose amount increases in the biggest fraction), dolomite ($\text{CaMg}(\text{CO}_3)_2$), ankerite, muscovite, chamosite and clinopyroxenes, all of them coming from the finest aggregates. Halite (NaCl) was also identified, confirming the presence of salts inside the mortars. The most interesting finding, though, regards the presence of minor amounts of brucite ($\text{Mg}(\text{OH})_2$), hydromagnesite ($\text{Mg}_5(\text{CO}_3)_4(\text{OH})_2 \cdot 4\text{H}_2\text{O}$) and magnesium silicates hydrates (M–S–H), which will be discussed later on.

5.4. Petrographic, chemical and mineralogical characterization of the pictorial layers

5.4.1. Optical microscopy

The thickness of the pictorial layers varies from different colour layers and ranges from 50 to 150 μm (e.g., Fig. 10a-c) but occasionally can be as thick as 200 μm in some regions when the surface below the painted layer is irregular (e.g., Fig. 10d-f). Red-coloured layers are more homogeneously distributed on the surfaces than other colours and occasionally deposited on rather flat surfaces such as in the case shown in Fig. 10a-c. Some painted layers show clear intermixing with the binder substrate (clearly seen in Fig. 10f). Green bands are also irregular but relatively homogenous in texture where cuprorivaite ($\text{CaCuSi}_4\text{O}_{10}$, confirmed by X-ray diffraction and EDS analyses, see below) is densely packed together with other minerals forming a continuous layer (Fig. 10g-i, sample #21).

The most distinctive feature of blue bands is the occurrence of relatively large aggregates of cuprorivaite that stand out of the surface (Fig. 10j-l, sample #22).

5.4.2. μ -XRD and EDS analyses

Micro X-ray diffraction performed on the surfaces of the mural samples revealed the presence of calcite and occasionally dolomite and quartz (see Table 3). The occurrence of halite in the X-ray diffraction patterns was dramatically decreased after treatment except in a few samples (see Table 3). The presence of ferric oxides and oxi-hydroxides

Table 2
Optical characterization of mortars.

Sample	Layer	Binder	Type	Aggregate Morphology	Grading	B:A	Porosity
2	1	Mainly calcitic	Siliceous (pyroxenes, olivine single grains, rarely serpentinized) 50 % and lime lumps 50 % (with occasional shrinking fissures)	Low sphericity and angular (siliceous aggregate) and high sphericity and sub-rounded (lumps)	Medium sorted	Low 1:5	Very high porosity with irregular shapes
	2	Mainly calcitic	Abundant dolomite grains and lime lumps, occasional cocchiopesto and very rare pyroxenes	Low sphericity and very angular (dolomite) and high sphericity and sub-rounded (lumps)	Bad sorting close to the surface	High 1:3	Low porosity
4	1	Mainly calcitic	Abundant pyroxene and olivine crystals 60 %, small rock fragments (partially serpentinized peridotite and microgabbro) 10 %, lime lumps 30 %	Low sphericity and very angular (dolomite) and high sphericity and sub-rounded (lumps)	Roughly unimodal for siliceous aggregate and larger sizes for the lumps	Low 1:5	High porosity with irregular shapes
	2	Mainly calcitic	Dolomite grains (and very rare calcite grains), rare pyroxenes, brown lime lumps and rare serpentinite fragments	Elongated and very angular dolomite grains, low sphericity and rounded lumps	Poor sorting	High 1:3	High porosity
8	1	Mainly calcitic	Pyroxene and rock grains (peridotite/gabbro), rare quartz grains, brown lumps, rare serpentinite fragments	Elongated and angular pyroxenes grains and well rounded quartz grains	Poor sorting	Medium 1:4	Rather low porosity
	2	Mainly calcitic	Exclusively dolomite grains	Low sphericity and very angular	Medium sorted	High 1:3 to 1:2	Low porosity with irregular shapes
13	1	Mainly calcitic	Large proportions of brown lumps and dolomite grains, pyroxene grains lumps in smaller proportions (rare calcite grains and peridotite/gabbro/serpentinite rock fragments)	Low sphericity and angular (siliceous aggregate) and high sphericity and sub-rounded (lumps)	Medium sorted and bimodal (large lumps and smaller size of the other aggregates)	Low 1:5	Medium porosity
	2	Mainly calcitic	Almost exclusively dolomite grains with only few grains of pyroxenes	Low sphericity and very angular	Medium sorted	High 1:2	Low porosity
14	1	Mainly calcitic	Quartz grains and brown lumps, rare pyroxenes	Low sphericity and sub-rounded (quartz aggregate) and high sphericity and sub-rounded (lumps)	Well sorted	High 1:3	Low porosity
	2	Mainly calcitic	Almost exclusively dolomite grains with only few grains of pyroxenes	Low sphericity and very angular	Medium sorted	High 1:2	Low porosity
15	1	Mainly calcitic	Mostly pyroxenes, olivine and lime lumps, occasional small rock fragments (oxide gabbro?)	Medium sphericity and very angular (pyroxenes) and high sphericity and sub-rounded (lumps)	Poor sorting	High 1:3	Low porosity with only few large pores
	2	Mainly calcitic	Exclusively dolomite grains	Low sphericity and very angular	Poor sorting	Low 1:5	Low porosity
16	1	Mainly calcitic	Abundant large lime lumps with pyroxenes, olivine, quartz (?) and dolomite grains, rare serpentinite fragments	Medium sphericity and very angular (pyroxenes) and high sphericity and sub-rounded (lumps)	Well sorted	Low 1:5	High porosity, some small rounded pores and large irregular pores
	2	Mainly calcitic	Exclusively dolomite grains	Low sphericity and very angular	Medium sorted	High 1:3 to 1:2	Medium porosity with irregular pores
17	1	Mainly calcitic	Very heterogenous, pyroxenes, rock fragments (including serpentinite), brown lime lumps, rare serpentinite fragments	Generally high sphericity and angular	Poor sorting	Low 1:5	Medium porosity with rounded pores
	2	Mainly calcitic	Exclusively dolomite grains	Low sphericity and very angular	Poor sorting	High 1:3	Medium porosity with large irregular pores
18	1	Mainly calcitic	Largely dominated by brown lumps and minor pyroxene fragments	High sphericity and sub-rounded (lumps) and low sphericity and angular (pyroxene fragments)	Poor sorting	High 1:3	High porosity with small rounded pores
	2	Mainly calcitic	Dominated by dolomite fragments but with relatively abundant cocchiopesto and lime lumps	Medium sphericity and highly angular (dolomite fragments)	Medium sorted	Medium 1:4	High porosity with small rounded pores
19	1	Mainly calcitic	Rock fragments from different origins (serpentinite, deformed calcitic marble, deformed gabbro/gneiss, deformed quartzite), minor pyroxenes, calcite fragments and lime lumps	Medium sphericity and rounded to sub-rounded	Poor sorting	High 1:3	Relatively low porosity
	2	Mainly calcitic	Very large proportion of lime lumps, cocchiopesto, minor pyroxenes	Medium sphericity and rounded to sub-rounded	Medium sorted	Medium 1:4	Medium porosity with large irregular pores
20	3	Mainly calcitic	Dominated by dolomite grains and lime lumps	Very low sphericity and very angular	Poor sorting	Medium 1:4	High porosity with irregular pores
	1	Mainly calcitic	Large brown lumps with minor dolomite and pyroxene grains, rare serpentinite fragments	High sphericity and sub-rounded (lumps) and low sphericity and angular (pyroxene and dolomite fragments)	Well sorted	Low 1:5	High porosity with irregular pores

(continued on next page)

Table 2 (continued)

Sample	Layer	Binder	Type	Aggregate Morphology	Grading	B:A	Porosity
	2	Mainly calcitic	Exclusively dolomite grains	Low sphericity and very angular	Poor sorting	Very high 1:2	Low porosity with small irregular and rounded pores
21	1	Mainly calcitic	Lime lumps, pyroxene, olivine fragments and rock fragments (serpentinite)	Low sphericity and sub-rounded (lumps) and high sphericity and sub-rounded (pyroxene)	Medium sorted	Low 1:5	Very high porosity with large irregular pores
	2	Mainly calcitic	Exclusively dolomite grains	Low sphericity and very angular	Poor sorting	Very high 1:2	Low porosity with small irregular and rounded pores
22	1	Mainly calcitic	Very heterogenous, rock fragments (gabbro, serpentinite, deformed quartzite, partially serpentinized olivine), pyroxene and rare dolomite fragments, Cocciopesto, unusually very small fragments of pyroxenes (?)	Some pyroxenes with high sphericity and very rounded	Bimodal sorting	High 1:3	Low porosity with few large irregular pores
	2	Mainly calcitic	Dominated by dolomite grains with minor partially serpentinized olivine fragments, rare cocciopesto and lumps	Low sphericity and very angular	Poor sorting	Very high 1:2	Low porosity with small irregular pores

(hematite and goethite) characterize red and yellow zones, respectively (Table 3, Fig. 11). Cinnabar was found only in very small quantities in sample #15 having a distinctive bright red colour (Table 3), the presence of many other phases with overlapping peaks in this sample makes however difficult to carry out a precise identification of this mineral phase.

X-ray diffraction clearly confirmed the occurrence of abundant cuprorivaite and quartz in both blue and green-coloured bands. Green bands also show the distinctive occurrence of ferro-magnesium phyllosilicates such as glauconite $((K,Na)(Fe^{3+},Al,Mg)_2(Si,Al)_4O_{10}(OH)_2)$, celadonite $(K(Mg,Fe^{2+})(Fe^{3+},Al)[Si_4O_{10}](OH)_2)$ and/or clinocllore $((Mg,Fe^{2+})_5Al(Si_3Al)O_{10}(OH)_8)$. These phyllosilicates are also present in blue colours. Graphite was detected in black zones while in white zones aragonite together with mica was widespread. The occurrence of minor amounts of micas and kaolinite has been noticed mostly in yellow and red bands.

EDS mapping of the pictorial layers (Fig. 12) confirms the chemical composition of the main minerals resulting in distinctive colours and further revealing the different morphology and contact relation between the paint layer and the mortar. Red bands (Fig. 12a and b) show sharp contacts with the mortar and a homogeneous distribution of iron proceeding from hematite (according to μ -XRD), together with quartz, K-feldspar and/or muscovite in the binder. The transition between the yellow-painted layer (with goethite and scarce hematite) and the mortar is more gradual (Fig. 12c).

EDS mapping of the green colour pigments confirms the homogenous distribution of quartz and cuprorivaite (Fig. 12d and e) and the distinctive morphology of large aggregates formed by acicular to prismatic cuprorivaite crystals mixed with quartz in the blue-painted zones (Fig. 12f). Fig. 12f further shows how the aggregates are inserted in the binder and covered by a more continuous layers of quartz and ferro-magnesian phyllosilicates that are not preserved in other areas of the sample, due to the delicate morphology of the cuprorivaite grains observed under the optical microscope (Fig. 10j-l).

6. Discussion

6.1. Mortars

At the investigated site, there is no systematic differences between the different colours of the pictorial layers and the mortars used for the preparation of the walls, showing that the same mortar preparation was adopted in all samples. At least two distinctive mortar layers have been observed in all investigated samples broadly corresponding to the classical *intonaco* (plaster s.s., c.f. Izzo et al., 2016) and *intonachino/marmorino* layers (preparation layer, c.f. Izzo et al., 2016), except for sample

#19 (Fig. 3) where three layers could be clearly distinguished. The third layer in this sample could be classified as *arriccio*. We infer that the used aggregates were sourced from nearby river sand based on the large diversity of lithologies of the rock fragments and their rounded shape. It is likely that this third layer was also present in all samples but it was not preserved because their coarser aggregates tend to be more prone to scaling. Although Roman wall paintings traditionally consist of several mortar layers according to the classical descriptions of Vitruvius and Pliny (up to six or seven, e.g. Piovesan et al., 2012; Izzo et al., 2016; Cerrato et al., 2021), it is well known that the number of preparation mortar layers is significantly reduced in most peripheral Roman cities. At most Hispanic Roman archaeological sites only three layers are usually identified (e.g., up to three layers in Bilbilis, Cerrato et al., 2021). Therefore, the Roman archaeological site of *Las Dunas* shares the same building techniques for wall paintings with other Hispanic sites, namely the use of up to three well-distinguished layers of decreasing aggregate size, finishing with an outer layer (*marmorino*) where the aggregate is very pure and almost exclusively consisting of coarse mono crystalline dolomite grains. The rare occurrence of *cocciopesto* and the homogenous composition of the aggregates in the *marmorino* layer from *Las Dunas* is a characteristic feature of the Roman wall painting technique and allows differentiating this layer from the *intonaco* layer where the *cocciopesto* is more abundant (e.g., in Campania Region, Southern Italy, Pagano et al., 2022). In agreement with other Roman sites where marble rock fragments are the most common aggregate in the *marmorino* layer (Pagano et al., 2022), the aggregate in this layer from *Las Dunas* is remarkably composed exclusively of dolomitic marble grains. The coarse grain size of the dolomite grains (0.5 to 1 mm, Fig. 7j and k) and their irregular shapes indicate that the source for the raw material used for the *marmorino* layer was carefully selected from a coarse, undeformed dolomitic marble that was crushed and sorted to the selected grain size. The western area of the Betic Chain is well known for its multitude occurrence of Roman quarries exploiting *marmorina*. These include several types of limestones and calcareous breccias from the Subbetic Zone (Ontiveros-Ortega et al., 2019) and more importantly marbles from the Internal Zones of the Betic Chain (Alpujarride Complex, c.f., Lapuente et al., 2022). In particular, there is a district marble area in Malaga from the *Sierra Blanca* and *Sierra de Mijas* with abundant dolomitic marbles (Lapuente et al., 2022) that are within ca. 30–60 km from the investigated Roman archaeological site of *Las Dunas*. It is very likely that any of these quarries provided the raw material for the aggregate of the *marmorino* layer. Based on the occurrence of some polysynthetic twins in the dolomite grains we tentatively suggest the quarries of *Alhaurín de la Torre* or *Monda* as a potential source rather than *Mijas* (where polysynthetic twins are very abundant), *Coñ* or *Alhaurín el Grande* (Lapuente et al., 2022). The latter locality is easily

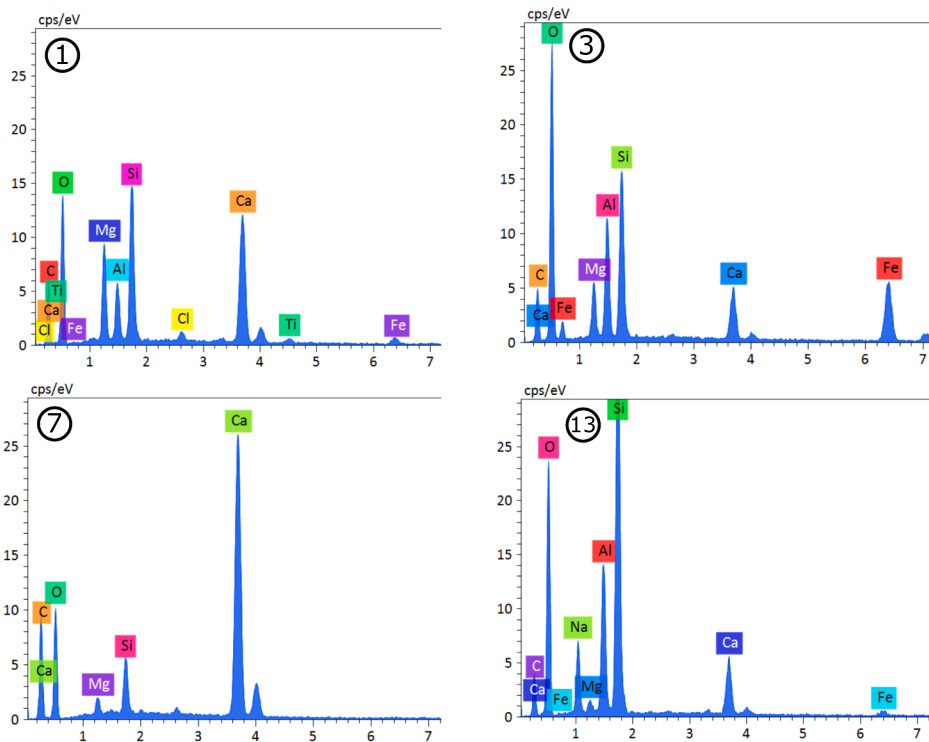
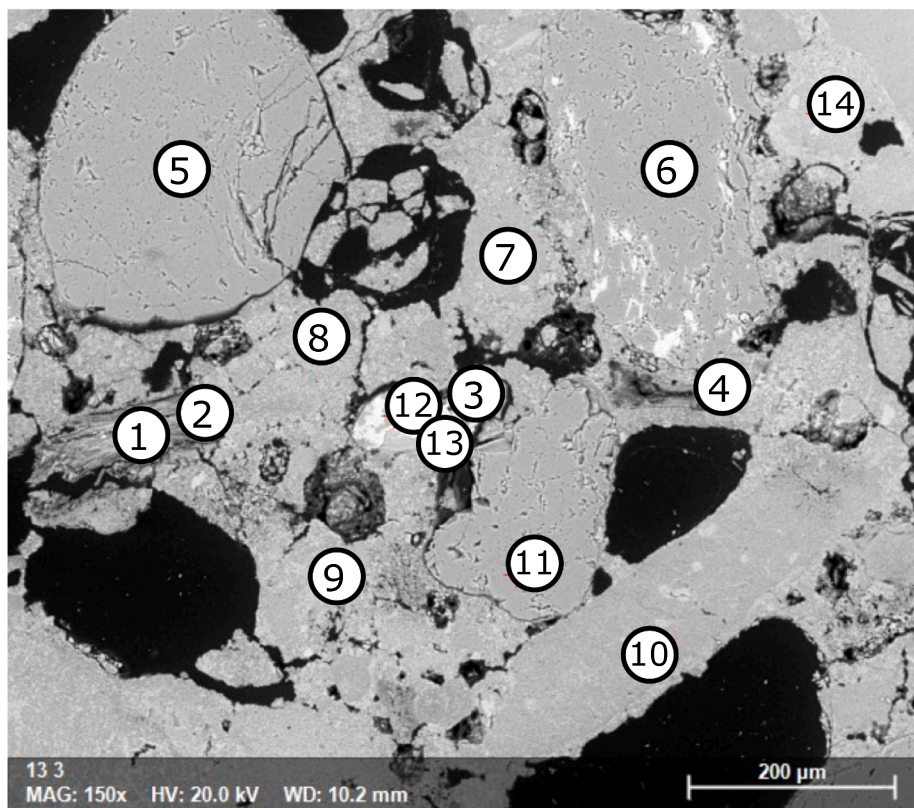


Fig. 8. Representative BSE of layer 1 (sample #13) with location of spots EDS analyses, some corresponding EDS spectra are shown here and the others in SM1. EDS spectrum 1, 2 and 4 (Ti-bearing clinopyroxene), 5, 6 and 11 (quartz), 7, 8, 9, 10 and 14 (calcitic binder containing Mg and Si), 3 and 12 (Fe-rich clinopyroxene), 13 (plagioclase).

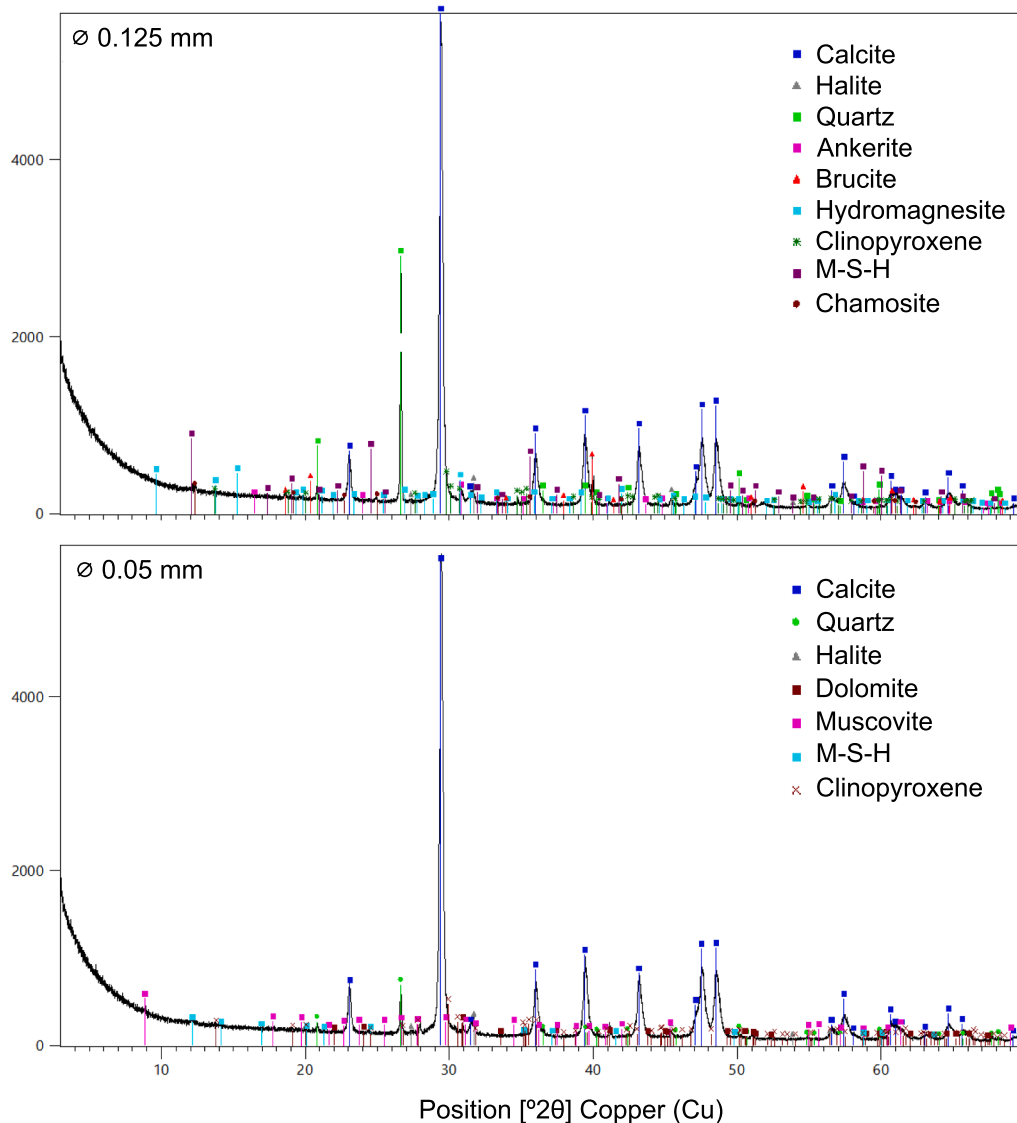


Fig. 9. Powder X-ray diffraction (XRD) of the binder for two sieved fractions (0.125 mm and 0.05 mm in diameter) after separation of the aggregate in sample #13. Note the occurrence of small amounts of brucite and hydromagnesite among other magnesian silicate phases.

discarded as it corresponds to calcitic marbles.

A singularity of the investigated mortars is the abundance of ultramafic grains forming the aggregates (mostly partially to fully serpentinized olivine and pyroxenes) making the mortars from the *Las Dunas* site rather unique among all Roman provinces. This is explained by the proximity of the archaeological site to the Ronda massif which exposed the largest ultramafic body worldwide (see [Jabaloy Sánchez et al., 2019](#) and references therein).

6.1.1. Nature and origin of the binder

The binder used in the mortars (and pictorial layers) is dominated by a calcite composition and can be in principle interpreted as the product of the carbonation of air-hardening lime binders. A closer inspection of the quantitative SEM-EDS analyses has revealed the systematic occurrence of small quantities of Mg and subordinate amounts of Si in both the binder and the lime lumps (Fig. 8 and SM2), under the form of the magnesian phases that can be all related to the use of a magnesian (or dolomitic) lime. Indeed, brucite, hydromagnesite (this one also observed under optical microscopy), and magnesian silicate hydrates were all identified by XRD (Fig. 9), even though the latter appear in very low amounts due to their poor crystallinity ([Diekamp et al., 2008](#)).

The presence of brucite in such ancient mortars might be surprising, even though magnesium hydroxide is known to show low reactivity towards carbonation ([Rodríguez-Navarro et al., 2023](#)) and therefore is not unlikely to be found in magnesian lime mortars ([Villaseñor and Price, 2008](#)). However, other factors might have played a role in the stabilization of this phase, as well as in the formation of magnesium silicates hydrates (M–S–H), possible due to the presence of Mg and subordinate amounts of Si in the lime (as observed in other Roman mortars, see [Dilaria et al., 2022](#); [Pagano et al., 2022](#)). It is worth remembering that archaeological wall painting fragments were found in a marine environment, reason why sodium chloride was found not only on the surface but also in the binder of the different mortar layers. As reported in [Karim et al. \(2017\)](#) sodium chloride gives place to an increase of pH in lime mortars, due to the formation of NaOH that in turns increases the solubility of silicates, thus promoting pozzolanic reactions that give place to hydrated silicates. Therefore, the precipitation of M–S–H in mortars from *Las Dunas* might have been promoted by the presence of NaCl, resulting in increased mortar strengths ([Karim et al., 2017](#)). At the same time, the precipitation of brucite might have been fostered by the formation of sodium hydroxide (as reported in [Bernard et al., 2019](#)).

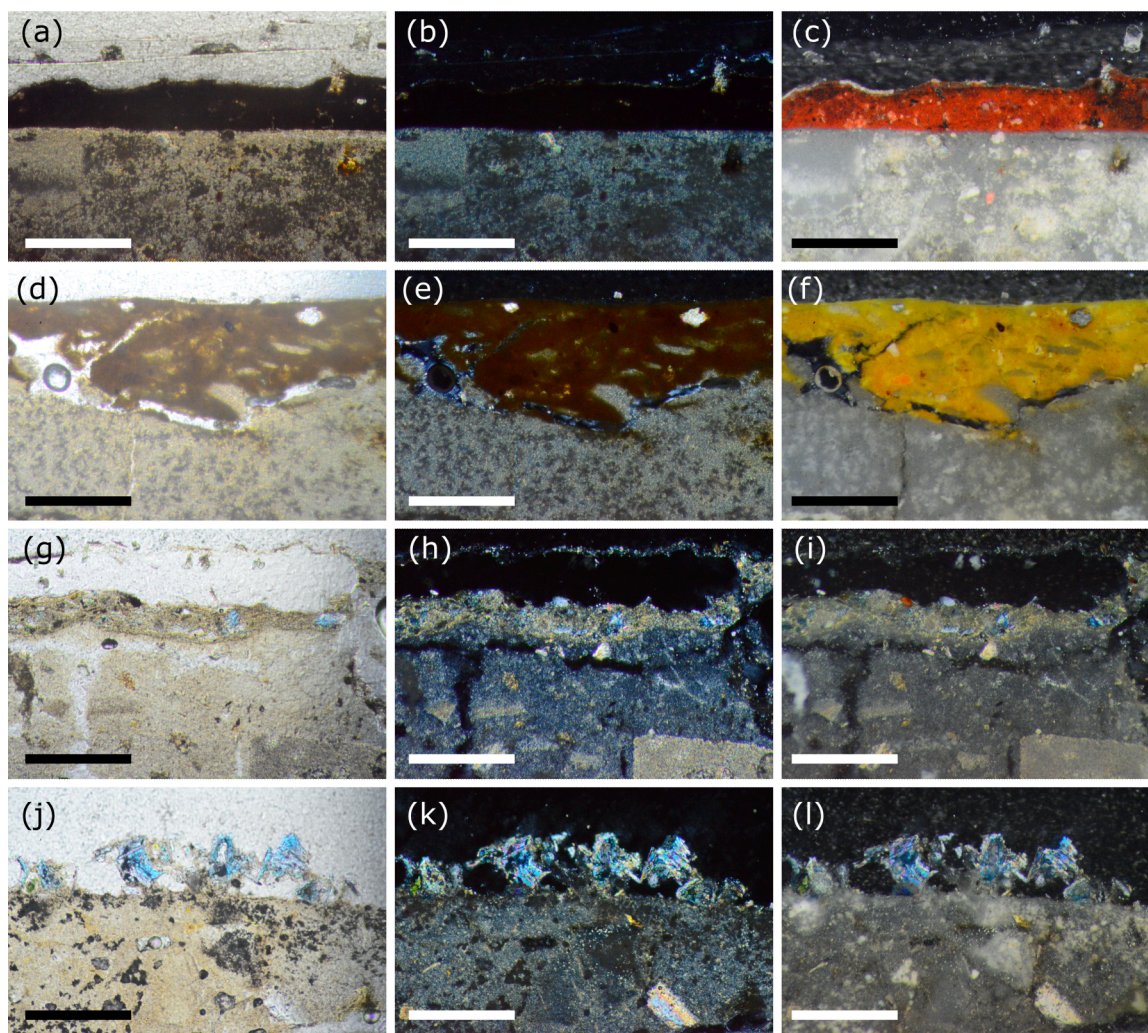


Fig. 10. Representative optical microscope images of the pictorial layer. The first and second rows are, respectively, plane and crossed polarized transmitted light images and in the third row are crossed polarized reflected images where colours are more easily distinguished. (a-c) Red colour (sample #13), note the homogeneity of the layer and the sharpness of the limit between the pictorial layer and the “intonaco”. (d-f) Yellow pictorial layer (sample #20) with variable thickness. Note the intermixing of between the pictorial layer and the lower binder for the mortar. (g-i) Thin (ca. 100 μm), green pictorial layer (sample #20), where a few dispersed cuprorivaite grains (50 μm) can be observed (c.f. Fig. 8g). (j-l) Discontinuous blue pictorial layer (sample #22) characterised by several large cuprorivaite acicular aggregates intermixed with quartz. All images are at the same scale where the bar represents 200 μm . (For interpretation of the references to colour in this figure legend, the reader is referred to the web version of this article.)

The location of the raw material source of the binder is difficult to assert but most likely originated from the multiple Roman quarries from the Subbetic Zone such as those of *Antequera* that exploited limestone where calcite was the main component (95–100 wt%) followed by minor amounts of quartz and traces of phyllosilicates, hematite, iron oxides, aragonite and siderite (Ontiveros-Ortega et al., 2019). The origin of Mg and Si could be ascribed to the minor silicate components in the limestone (mostly quartz and muscovite, see compositional range for the limestone expanding towards muscovite and quartz in Fig. 13) potentially used as raw material for the preparation of the lime. Available XRF bulk chemical data of Roman *marmora* quarries closest to the *Las Dunas* site (*Antequera-Teba-Ronda-Valle del Abdalajís* sector quarries, Ontiveros-Ortega et al., 2019) indicate however that the amount of MgO although variable (0.18–0.61 wt%), with an average 0.34 wt% is too low to explain the observed Mg content in the binder. In particular, the Mg/Ca in the limestone ranges from 0.005 to 0.016 mol ratio with an average of 0.009 whereas in the binder the Mg/Ca ranges from 0.019 to 0.069 with an average of 0.057 mol ratios (Fig. 13).

This suggests that the observed Mg/Ca ratio might have increased by intentionally adding powdered dolomite to the limestone, whereas the

minor Si content observed in the binder is compatible with the Si abundance in the limestone, which represents the main component of the lime. Mass balance estimations (grey solid lines in Fig. 13) suggest that the added dolomite component to the limestone represents up to 15 wt%, with an average value of 10 %. Interestingly the measured binder composition is relatively homogenous except for one analysis with the lowest Mg content that might correspond with pure limestone (Fig. 13). It is interesting to note that the binder composition plot outside any mixing between the limestone (calcite) and the peridotite (represented as dashed lines in Fig. 13) or any other common minerals observed as aggregate, such serpentized olivine, pyroxenes, muscovite or quartz.

Based on other studies on Roman mortars (Bertolini et al., 2013; Montana et al., 2018), it is not hard to believe that Romans from Baetica had intentionally added powdered dolomite marble to the limestone to obtain a magnesian (or dolomitic) lime, especially taking into account that both raw materials were available in the geological context of the site (Alpujarride Complex, Fig. 1). It is well known, indeed, that magnesian lime mortars exhibit higher plasticity (Arizzi and Cultrone, 2012; Arizzi et al., 2012) and mechanical strengths (Dheilly et al., 1999; Chever et al., 2010; Álvarez et al., 2021) compared to calcitic lime

Table 3
Identified minerals by micro X-ray diffraction in the pictorial layers.

	Name	Calcite (CaCO ₃)	Halite (NaCl)	Quartz (SiO ₂)	Dolomite (MgCaCO ₃)	Aragonite (CaCO ₃)	Hematite (Fe ₂ O ₃)	Goethite (FeO ₂ H)	Gypsum (CaSO ₄ ·2H ₂ O)	Muscovite KAl ₂ (AlSi ₃ O ₁₀) (OH) ₂	Kaolinite Al ₂ Si ₂ O ₅ (OH) ₄	Graphite (C)	Cuprorivaite (CaCuSi ₄ O ₁₀)	Cinnabar (HgS)	Glauconite	Chlorite	
White	1 white band	X	X	X		X			X								
	2 white band	X		X	X	X											
	8 white band	X		X	X	X					X						
	9 white band	X		X	X	X											
	11 white band	X		X		X											
	15 white band	X	X	X	X	X				X							
	23 white band	X			X	X				X							
	25 white band	X		X	X	X							X				
	27 white zone	X	X	X	X	X											
	Yellow	2 yellow band	X		X	X			X		X	X					
		9 yellow band	X		X				X		X	X					
10 yellow		X	X	X				X		X	X						
11 yellow band		X		X		X		X		X							
12 yellow band		X	X	X				X		X	X						
15 yellow band		X	X	X	X			X		X	X						
24 yellow zone		X		X	X	X				X							
25 yellow zone		X	X	X				X		X							
Red		1 red zone	X	X	X			X		X	X						
		2 red band	X		X		X	X			X						
	8 red band	X		X	X			X							X		
	9 red zone	X	X	X	X		X	X									
	12 red zone	X	X	X			X			X							
	13 red zone	X	X	X			X			X							

(continued on next page)

Table 3 (continued)

Name	Calcite (CaCO ₃)	Halite (NaCl)	Quartz (SiO ₂)	Dolomite (MgCaCO ₃)	Aragonite (CaCO ₃)	Hematite (Fe ₂ O ₃)	Goethite (FeO ₂ H)	Gypsum (CaSO ₄ ·2H ₂ O)	Muscovite KAl ₂ (AlSi ₃ O ₁₀) (OH) ₂	Kaolinite Al ₂ Si ₂ O ₅ (OH) ₄	Graphite (C)	Cuprorivaite (CaCuSi ₄ O ₁₀)	Cinnabar (HgS)	Glauconite	Chlorite
15 red zone	X	X	X	X		X			X	X			X		
23 red band	X		X	X		X									
24 red zone	X		X	X		X									
25 red zone	X	X	X			X									
27 red zone	X		X	X		X	X								
28 red zone	X	X	X	X		X									X
Green 8 green band	X		X									X		X	
11 green zone	X		X					X				X		X	
15 green zone	X		X	X								X		X	X
28 green zone	X	X	X	X	X									X	X
Blue 6 blue	X		X									X			
22 blue	X		X									X			
23 blue band	X		X	X				X				X			
26 blue	X		X									X			
Black 2 black zone	X		X		X			X		X	X				
8 black zone	X		X	X	X						X				
9 black zone	X	X	X	X							X				

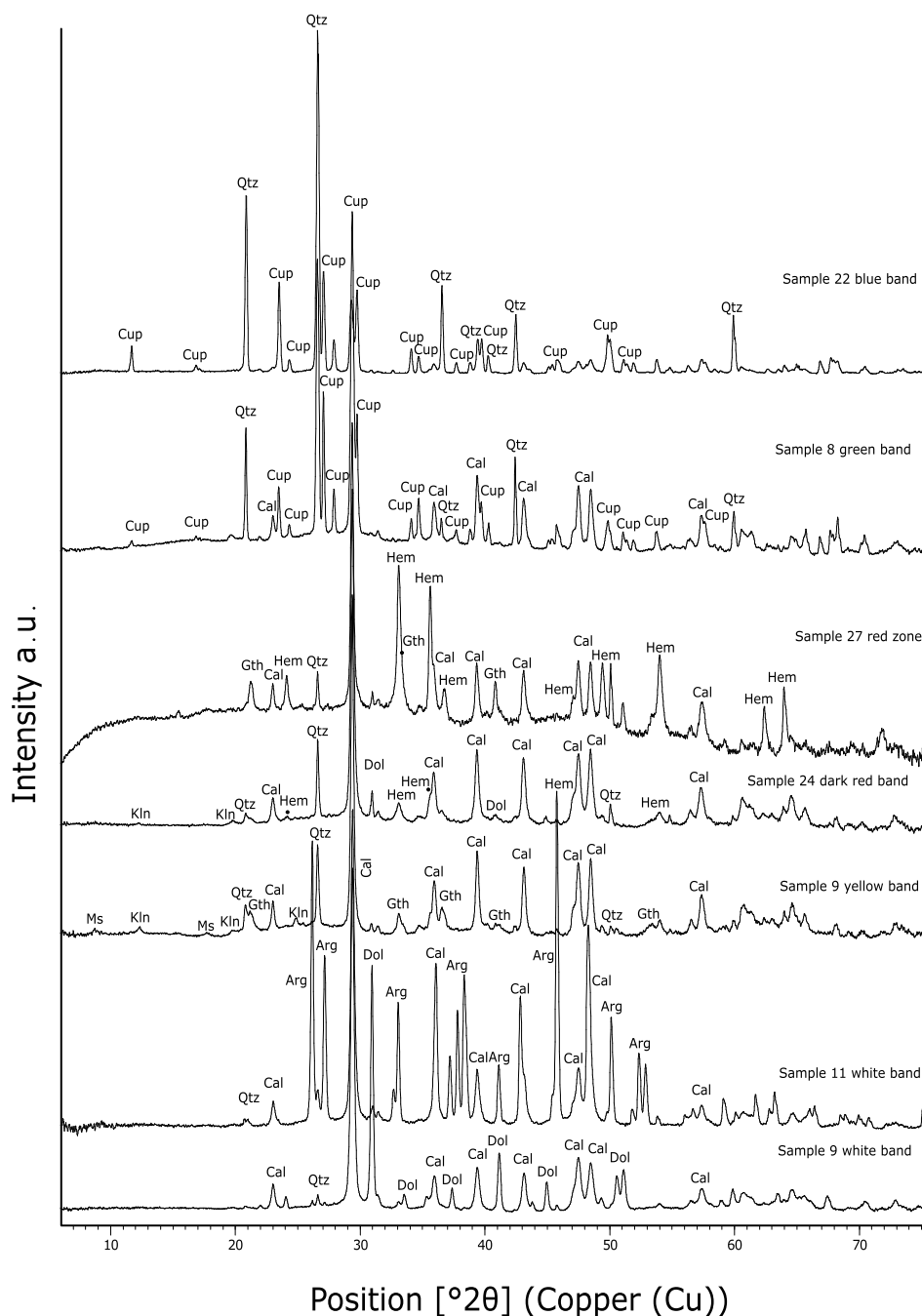


Fig. 11. Selected micro X-ray diffractograms from the pictorial surfaces for red, yellow, green, blue and white coloured areas.

mortars, due to the feeble hydraulicity conferred by magnesian limes (Chever et al., 2010).

These findings highlight the complex and varied approaches that ancient Roman craftsmen employed in creating durable and resilient mortars, underscoring the remarkable level of technological sophistication achieved by this ancient civilization.

6.2. Pictorial layers

Identified colours generically classified in this work as red, yellow, green, blue, black and white (Fig. 5) can, based on their mineralogical and chemical composition, be readily compared to classical Roman pigments, namely *red ochre* (hematite, Fe_2O_3), *yellow ochre* (goethite $\text{FeO}(\text{OH})$ and minor hematite), *green earth* (ferro-magnesian silicate minerals belonging to the mica group such as celadonite/glaucoune/

clinochlore), *Egyptian blue* (cuprorivaite, $\text{CaCuSi}_4\text{O}_{10}$), *carbon black* (graphitic carbon, C) and *lime-white* (aragonite, CaCO_3) respectively (Siddall, 2018). The use of aragonite for the white colours has been also described in other Roman sites (Villar and Edwards, 2005; Fuchs and Bearat, 1997; Varian and Bearat, 1997) and interpreted as ground marine shells. Different green hues were obtained by mixing different proportions of green earth pigments with cuprorivaite, a technique already described in other Roman wall paintings (Bugini and Folli, 1997; Gutman et al., 2016). Darker red or purple colours (*burgundy*) produced by addition of carbon and cuprorivaite to hematite reported in other Roman sites (e.g., Cerrato et al., 2021; Fuchs and Bearat, 1997) were not observed. Minium (Pb_3O_4) and/or lead oxide (PbO_2) were not observed neither in any of the yellow fragment.

The colour combinations observed at *Las Dunas* site correspond to the classical combinations described by Pliny (Gutman et al., 2016;

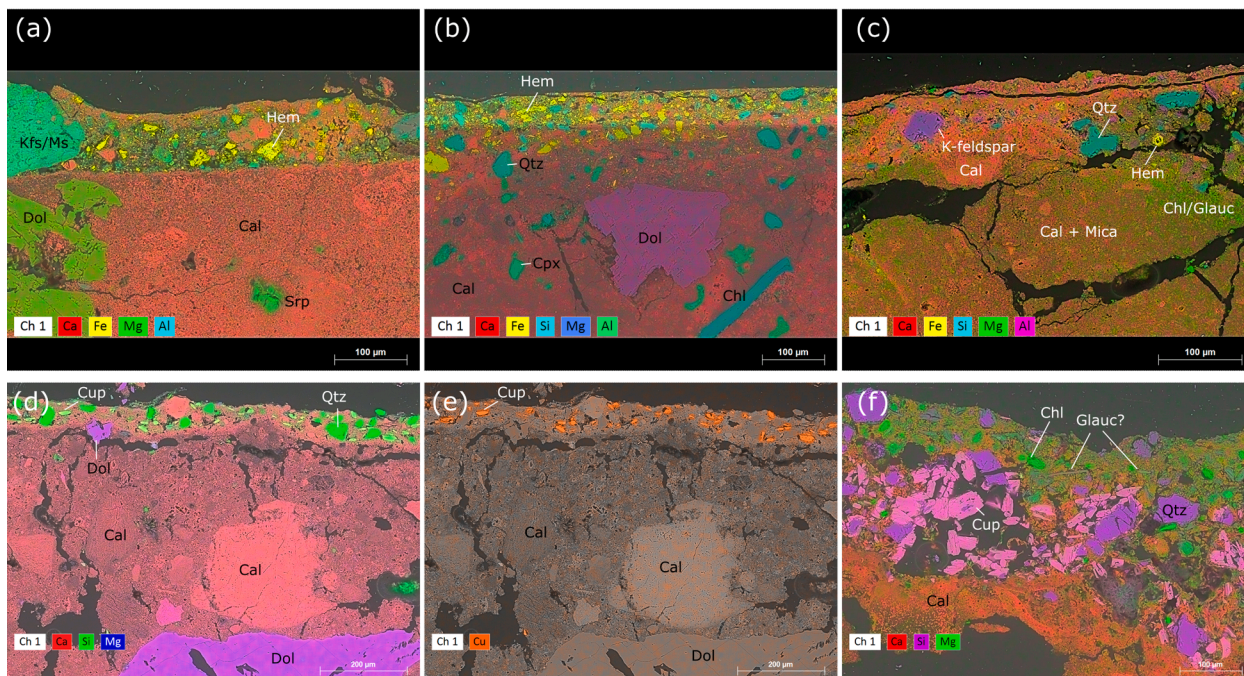


Fig. 12. EDS mapping of pictorial layers. The false colours are formed by the combination of several elemental distributions specified for each map, background images are secondary electron images. Because different elements were used for each map, the same minerals have different colours accordingly. Red colours (a) sample #13 and (b) sample #18, yellow colours (c) sample #20, green colours (d) and (e) sample #19, the location of cuprorivaite is highlighted in the Cu distribution map (e), blue colour (f) showing the cuprorivaite and quartz aggregate. Sample #21. (For interpretation of the references to colour in this figure legend, the reader is referred to the web version of this article.)

Guglielmi et al., 2020; Bracci et al., 2022; Siddall, 2018; López-Martínez et al., 2016). Similar colour palette has been reported from other archaeological sites from Hispania (Moreno et al., 1997; Edreira et al., 2001, 2003; Villar and Edwards, 2005; Fernández Rodríguez and Fernández Fernández, 2005; López-Martínez et al., 2016). More expensive and rare pigments such as malachite ($\text{Cu}_2(\text{CO}_3)(\text{OH})_2$) or azurite ($\text{Cu}_3(\text{CO}_3)_2(\text{OH})_2$) were not observed, with the possible exception of some traces of cinnabar (HgS) detected by μ -XRD in one sample (#15). It is worth to note that cinnabar was probably available as it is well-known in mural paintings from other Hispanic Roman provinces (Edreira et al., 2001, 2003, Villar and Edwards, 2005; Tsantini et al., 2018) given the many cinnabar ore mines in Spain, notably *Almadén* (Tsantini et al., 2018).

Most paint layers consist of only one colour, but some samples show clear evidence of two colour layers. For instance, in sample #15 a yellow layer was first applied followed by a green coloured layer while in sample #8 the reverse colour sequence has been observed. More complex stratigraphies of paint layers have been also identified such as in sample #14 where a red layer is followed by white layer that is finished on top with a very thin red layer.

The painting technique observed in *Las Dunas* varies between the different colours. Yellow pigments are always intermingled with the preparation mortar (*marmorino*) and therefore are interpreted as applied following the *fresco* technique. The application of red pigments seems to be more diverse. Some red samples show clear straight contacts with the preparation mortar (sample #13) that are interpreted to be applied when the preparation mortar was already dry, which would correspond either to a *secco* or *mezzo fresco*. In both painting techniques, pigments are applied onto a dry plaster, with the difference that in the former they are mixed with an organic binder whilst in the latter they are mixed with slaked lime or limewater, reason why the *mezzo fresco* is also defined “lime-paint” (Piovesan et al., 2012). According to literature (Casadio et al., 2004; Casoli, 2021), the identification of an organic binder by means of chemical analytical techniques (e.g. Raman, FT-IR and pyrolysis-gas chromatography/mass spectroscopies) could enable

distinguish between one technique or another. However, due to the precarious state of conservation of the samples studied, it is most likely that, even though an organic binder was used, this would have suffered partial or total degradation over time, making difficult to reveal its presence. Under these conditions, chemical analyses might not be conclusive, and for this reason they were discarded in this study, opting instead to focus our attention on the micro-textural differences observed in the samples stratigraphy by means of optical and electron microscopies (c.f. Piovesan et al., 2012). Backscattered images of a red sample (#13) reveal the occurrence of a very thin (ca. 10 μm) brighter layer in agreement with the experimental results of Piovesan et al. (2012) that identified this thin layer as carbonation layer in the plaster immediately underneath the painted layer in the lime-painting technique. The existence of this thin carbonation layer strongly suggests that the plaster from the preparation mortar was already dry when the lime-paint was applied. Other red-coloured samples show characteristics of the *fresco* technique (sample #4), or a temporal evolution during the wall painting that started as *fresco* but finished as lime-paint (i.e. *mezzo fresco*) (sample #18). Green and blue pigments are interpreted to be invariably applied using the *fresco* technique although the penetration of the cuprorivaite and quartz crystals in the preparation mortar is very limited. Moreover, the mixing between green and blue pigments differs among samples, with cases where cuprorivaite and quartz are dispersed within the green-coloured mica group minerals and in others where the two pigments form different layers (Fig. 12f).

Quantitative colour measurements of the investigated fragment surfaces after treatment (Fig. 6) closely resemble other works (Fernández Rodríguez and Fernández Fernández, 2005; Pérez-Rodríguez et al., 2015; Pagano et al., 2022) and highlights the importance of cleaning technique when comparing the results from other studies.

7. Conclusions

The Roman mural paintings are characterized by a high degree of consistency in the recipes and techniques used for their execution.

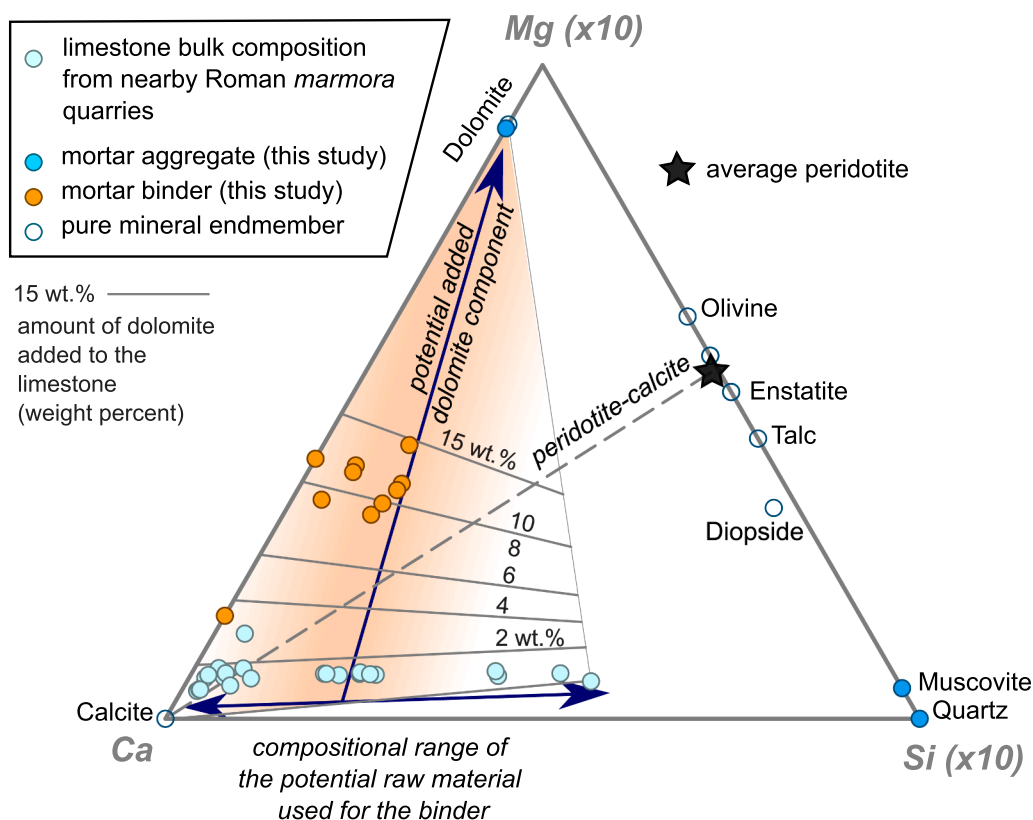


Fig. 13. CMS (Ca-Mg-Si) compositional diagram in mol proportions showing the composition of the binder observed in a representative sample (sample #13) based on quantitative SEM-EDS analyses. Also plotted are the bulk rock composition of limestones from nearby Roman quarries (Ontiveros-Ortega et al., 2019) and pure dolomite. Analysed binders from Las Dunas plots in a mixing line between these two compositions approximately corresponding up to 15 wt% of dolomite added to the raw limestone used for the preparation of the magnesian (dolomitic) lime. Other mineral endmembers are also plotted for comparison, but they do not show mixing trends with the binder (particularly there is no mixing between calcite and a peridotite bulk composition represented with a solid star). Mg and Si are multiplied by a factor of 10 to better depict the compositional variability of the binder. Compositional diagram computed with Cspace (Torres-Roldán et al., 2000).

However, slight variations in the techniques are known to occur, often due to the availability of local raw materials.

The mineralogical and compositional characterization of the wall painting fragments recovered at the archaeological site from *Las Dunas* (San Pedro de Alcántara, Malaga, S Spain) reveals the similarities in the colour palette (including the use of one of the first synthetic pigments known as *Egyptian blue*) relative to other Roman sites in the Iberian Peninsula. Moreover, the detailed optical microscopic observations and EDS mapping allow to distinguish the use of at least two different painting techniques depending on the applied colour: the *fresco* and the *mezzo fresco* (or “lime-paint”) technique. The use of one painting technique over the other was most likely related to the different physical and mechanical properties of the pigments that are eventually related to their mineralogical composition and grain size.

This study shows a rather unique feature of the mortars, where abundant silicates and ferromagnesian silicates (mostly quartz, pyroxenes and partially or completely serpentinized olivine from the nearby Ronda Peridotite massif in Malaga) were used as aggregates of the mortar to give rise to mortars with primitive hydraulic features, suggesting a connection between the availability of raw materials and the techniques used by Roman craftsmen. Additionally, it is possible to confirm, based on the chemical analyses of the binder that a magnesian (dolomitic) lime was used, and that it was obtained by adding an extra component of dolomitic marble (ca. 10 wt%) to the raw material (most likely limestones from nearby Roman quarries).

The availability of these raw materials could have been explored to obtain more workable, resistant and durable mortars. Future detailed characterization of Roman mortars in other archeological sites from Baetica will allow to confirm if the use of magnesian lime mortars with

feeble hydraulicity as observed in *Las Dunas* site was widespread or restricted to the sites near the natural occurrence of the specific raw material required for their manufacturing (Ronda Peridotite massif in Malaga).

Overall, we can conclude that the use of a magnesian lime, together with cocciopesto and ferromagnesian silicates, confirms that Romans were able to obtain hydraulic mortars even though volcanoclastic materials were not locally available for this purpose, as in other areas of the Roman empire (Artioli et al., 2019).

The marine environment, finally, might have played an important role in the development of the hydrated phases, further promoting the mortar strength increase.

Our findings highlight the complex and varied approaches that ancient Roman craftsmen employed in creating durable and resilient mortars, underscoring the remarkable level of technological sophistication achieved by this ancient civilization. Not less important, this study highlights the relevance of considering local geology and raw material availability when studying ancient artifacts and their production techniques. Furthermore, it emphasizes the potential for utilizing geological knowledge to gain a deeper understanding of the technological advancements and cultural practices of past civilizations.

CRediT authorship contribution statement

M. Urosevic: Methodology, Formal analysis, Data curation, Investigation, Writing – original draft. **D. Jiménez-Desmond:** Formal analysis, Investigation. **A. Arizzi:** Conceptualization, Visualization, Investigation, Funding acquisition, Project administration. **J.S. Pozo-Antonio:** Funding acquisition. **C. Moreno Prieto:** Funding acquisition.

M. Vila Oblitas: Writing – original draft.

Declaration of Competing Interest

The authors declare that they have no known competing financial interests or personal relationships that could have appeared to influence the work reported in this paper.

Data availability

Data will be made available on request.

Acknowledgements

M. Urosevic and A. Arizzi were supported by State Research Agency (SRA) and the Ministry of Science and Innovation under the Research Project PID2020-119838RA-I00, within the Junta de Andalucía Research Group RNM179. D. Jimenez-Desmond and J.S. Pozo-Antonio were supported by the Ministry of Science and Innovation, Government of Spain through the project RYC2020-028902-I. The authors thank to J.A. Padrón-Navarta for his petrological input and to archeologists A. León Sierra, I. Gómez Montenegro, J. García Calvente, E. Loriguillo Millán, J. Aragón Jiménez and M. Requena Cueto for their work at the archaeological site *Las Dunas*. Authors also thank A. Dorado Alejos of the Dpt. Of Prehistory and Archaeology of the University of Granada, for his assistance in the use of the Coxem EM-30AXP low vacuum SEM (equipment funded by the project EQC2018-004880-P).

Appendix A. Supplementary data

Supplementary data to this article can be found online at <https://doi.org/10.1016/j.jasrep.2023.104280>.

References

- Abad Casal, L., 1982. La pintura romana en España. Universidad de Alicante, Universidad de Sevilla, Spain <http://hdl.handle.net/10045/21902>.
- Alayón, J., Girón, S., Romero-Odero, J.A., Nieves, F., 2021. Virtual sound field of the Roman theatre of Malaca. *Acoustics* 3 (1), 78–96. <https://doi.org/10.3390/acoustics3010008>.
- Alcántara, G.C., Díaz, A.F., Hidalgo, D.C., Arrebola, J.R.R., 2022. A compositional and archaeometric study of the Third Pompeian Style located at the Mons Saturnus of Carthago Nova (Cartagena, España). *J. Archaeol. Sci. Rep.* 46, 103670. <https://doi.org/10.1016/j.jasrep.2022.103670>.
- Aliatis, I., Bersani, D., Campani, E., Casoli, A., Lottici, P.P., Mantovan, S., Marino, I.G., Ospitali, F., 2009. Green pigments of the Pompeian artists' palette. *Spectrochim. Acta A Mol. Biomol. Spectrosc.* 73 (3), 532–538. <https://doi.org/10.1016/j.saa.2008.11.009>.
- Aliatis, I., Bersani, D., Campani, E., Casoli, A., Lottici, P.P., Mantovan, S., Marino, I.G., 2011. Pigments used in Roman wall paintings in the Vesuvian area. *J. Raman Spectrosc.* 41 (11), 1537–1542. <https://doi.org/10.1002/jrs.2701>.
- Álvarez, J.L., Veiga, R., Martínez-Ramírez, S., Secco, M., Faria, P., Maravelaki, P.N., Ramesh, M., Papayanni, I., Válek, J., 2021. RILEM TC 277-LHS report: a review on the mechanisms of setting and hardening of lime-based binding systems. *Mater. Struct.* 54, 63.
- Arizzi, A., Cultrone, G., 2012. The difference in behaviour between calcitic and dolomitic lime mortars set under dry conditions: The relationship between textural and physical-mechanical properties. *Cem. Concr. Res.* 42, 818–826. <https://doi.org/10.1016/j.cemconres.2012.03.008>.
- Arizzi, A., Hendrickx, R., Cultrone, G., Van Balen, K., 2012. Differences in the rheological properties of calcitic and dolomitic lime slurries: Influence of particle characteristics and practical implications in lime-based mortar manufacturing. *Mater. Constr.* 62, 231–250. <https://doi.org/10.3989/mc.2011.00311>.
- Artioli, G., Secco, M., Addis, A., 2019. The Vitruvian legacy: Mortars and binders before and after the Roman world. *EMU Notes in Mineralogy* 20 (4), 151–202.
- Bagnall, R.S., Brodersen, K., Champion, C.B., Erskine, A., Huebner, S.R., 2013. *The Encyclopedia of Ancient History*, 1. Wiley-Blackwell.
- Belén, M., Birley, A., Caballos Rufino, A., Chaves Tristán, F., Domergue, C., Downs, M., Escacena, J.L., Keay, S., León, P., Márquez, C., Mayer, M., Ponsich, M., Remesal Rodríguez, J., Rodà, I., Stylow, A., Ventura, A., 1998. The archaeology of early Roman Baetica. *Journal of Roman Archaeology*. Portsmouth, Rhode Island.
- Beltrán Fortes, J., Loza Azuaga, Ontiveros Ortega, E., Rodríguez Gutiérrez, O., Taylor, R., 2011. La explotación y el empleo de "marmorata" en la Baetica. Un proyecto de investigación de base arqueométrica. *Itálica: revista de arqueología clásica de Andalucía* 1, 51–75.
- Benloch, P.O., 2006. La preparación de la pintura mural en el mundo romano. *Ex Novo Revista D'història i Humanitats* 23–40.
- Bergamonti, L., Cirilini, M., Graiff, C., Lottici, P.P., Palla, G., Casoli, A., 2022. Characterization of waxes in the Roman wall paintings of the Herculaneum Site (Italy). *Appl. Sci.* 12 (21), 11264. <https://doi.org/10.3390/app122111264>.
- Bernard, E., Lothenbach, B., Pochard, L., Cau-Dit-Coumes, C., 2019. Alkali binding by magnesium silicate hydrates. *J. Am. Ceram. Soc.* 102, 6322–6336.
- Bertolini, L., Carsana, M., Gastaldi, M., Lollini, F., Redaelli, E., 2013. Binder characterisation of mortars used at different ages in the San Lorenzo church in Milan. *Mater. Charact.* 80, 9–20.
- Bracci, S., Cantisani, E., Conti, C., Magrini, D., Vettori, S., Tomassini, P., Marano, M., 2022. Enriching the knowledge of Ostia Antica painted fragments: A multi-methodological approach. *Spectrochimica Acta - Part a: Molecular and Biomolecular Spectroscopy* 265. <https://doi.org/10.1016/j.saa.2021.120260>.
- Bugini, R., Folli, L., 1997. Materials and making techniques of Roman Republican wall paintings (Capitolium, Brescia, Italy). In: Bearat, H., Fuchs, M., Maggetti, M., Paunier, D. (Eds.), *Roman Wall Painting: Materials, Techniques, Analyses and Conservation*, *Proceedings of the International Workshop*, Fribourg 7-9 March 1996., Institute of Mineralogy and Petrology, Fribourg University, pp. 121–130.
- Calabria Salvador, I., Zalbidea Muñoz, A., 2019. Estudio de las pinturas murales de la sala del Mosaico de los Amores de la ciudad fibero-romana de Cástulo. *Geoconservación* 16, 45–61. <https://doi.org/10.37558/gec.v16i0.663>.
- Cánovas Ubera, A., 1999. Un nuevo proyecto arqueológico en Colonia Patricia Corduba. La pintura mural. *Anales de Arqueología Cordobesa* 161–175. <https://doi.org/10.21071/aac.v0i1.1281>.
- Casadio, F., Giangualano, I., Piqué, F., 2004. Organic materials in wall paintings: the historical and analytical literature. *Stud. Conserv.* 49 (sup1), 63–80. <https://doi.org/10.1179/sic.2004.49.Supplement-1.63>.
- Casoli, A., 2021. Research on the organic binders in archaeological wall paintings. *Appl. Sci.* 11 (19), 9179. <https://doi.org/10.3390/app11199179>.
- Cerrato, E.J., Iniguez, L., Cosano, D., Guiral, C., Ruiz, J.R., 2021. Multi-analytical identification of a painting workshop at the Roman archaeological site of Bilbilis (Saragossa, Spain). *J. Archaeol. Sci. Rep.* 38. <https://doi.org/10.1016/j.jasrep.2021.103108>.
- Cerrato Moreno, E.J., 2021. *Archaeometric study of roman wall painting in Córdoba*. University of Cordoba, Spain. Doctoral dissertation.
- Chever, L., Pavia, S., Howard, R., 2010. Physical properties of magnesium lime mortars. *Mater. Struct.* 43, 283–396.
- Cortea, I.M., Ratoiu, L., Ghervase, L., Țentea, O., Dinu, M., 2021. Investigation of ancient wall painting fragments discovered in the roman baths from alburnus maior by complementary non-destructive techniques. *Appl. Sci.* 11 (21), 10049. <https://doi.org/10.3390/app112110049>.
- Cuní, J., 2016. What do we know of Roman wall painting technique? Potential confounding factors in ancient paint media analysis. *Heritage Science* 4 (1), 1–13. <https://doi.org/10.1186/s40494-016-0111-4>.
- DeLaine, J., 2021. Production, transport and on-site organisation of Roman mortars and plasters. *Archaeol. Anthropol. Sci.* 13 (11), 1–17. <https://doi.org/10.1007/s12520-021-01401-5>.
- Dheilly, R.M., Bouguerra, A., Beaudoin, B., Tudo, J., Queneudec, M., 1999. Hydromagnesite development in magnesian lime mortars. *Mater. Sci. Eng. A* 268, 127–131.
- Diekamp, A., Konzett, J., Wertl, W., Tessadri, R., Mirwald, P.W., 2008. Dolomitic lime mortars – a commonly used building material for medieval buildings in western Austria and northern Italy. In: Lukaszewicz, J.W., Niemcewicz, P. (Eds.), *Proceedings of the 11th International Congress on Deterioration and Conservation of Stone*, Torun, Poland, vol. I, pp. 597–604.
- Diekamp, A., Konzett, J., Mirwald, P.W., 2009. Magnesian lime mortars – identification of magnesium-phases in medieval mortars and plasters with imaging techniques. In: Middendorf, B., Just, A., Klein, D., Glaubitt, A., Simon, J. (Eds.), *Proceedings of the 12th Euroseminar on Microscopy Applied to Building Materials*. Dortmund, Germany, pp. 309–317.
- Dilaria, S., Secco, M., Rubinić, M., Bonetto, J., Miriello, D., Barca, D., Artioli, G., 2022. High-performing mortar-based materials from the late imperial baths of Aquileia: An outstanding example of Roman building tradition in Northern Italy. *Geoarchaeology* 37 (4), 637–657. <https://doi.org/10.1002/gea.21908>.
- Durán, A., Perez-Rodríguez, J.L., De Haro, M.J., Franquelo, M.L., Robador, M.D., 2011. Analytical study of Roman and Arabic wall paintings in the Patio De Banderas of Reales Alcázares' Palace using non-destructive XRD/XRF and complementary techniques. *J. Archaeol. Sci.* 38 (9), 2366–2377. <https://doi.org/10.1016/j.jas.2011.04.021>.
- Edreira, M.C., Feliu, M.J., Fernández-Lorenzo, C., Martín, J., 2001. Roman wall paintings characterization from Cripta del Museo and Alcazaba in Mérida (Spain): chromatic, energy dispersive X-ray fluorescence spectroscopic, X-ray diffraction and Fourier transform infrared spectroscopic analysis. In: *Anal. Chim. Acta* 434.
- Edreira, M.C., Feliu, M.J., Fernández-Lorenzo, C., Martín, J., 2003. Spectroscopic analysis of roman wall paintings from Casa del Mitreo in Emerita Augusta, Mérida. Spain. *Talanta* 59 (6), 1117–1139. [https://doi.org/10.1016/S0039-9140\(03\)00020-1](https://doi.org/10.1016/S0039-9140(03)00020-1).
- Fear, A.T., 1996. *Rome and Baetica: Urbanization in Southern Spain* c. Oxford University Press Inc., New York.
- Fernández Rodríguez, J.M., Fernández Fernández, J.A., 2005. Application of the second derivative of the Kubelka-Munk function to the semi-quantitative analysis of Roman paintings. *Color Res. Appl.* 30 (6), 448–456. <https://doi.org/10.1002/COL.20157>.
- Giménez Rodríguez, M., 2021. Análisis arqueológico de la pintura mural de cronología tardorromana localizada en la provincia de la Bética. *Arqueología y Territorio*, No 18, 45–55. <https://doi.org/10.5281/6226431>.

- Guglielmi, V., Comite, V., Andreoli, M., Demartin, F., Lombardi, C.A., Fermo, P., 2020. Pigments on roman wall painting and stucco fragments from the Monte d'Oro Area (Rome): A multi-technique approach. *Applied Sciences (switzerland)* 10 (20), 1–18. <https://doi.org/10.3390/app10207121>.
- Gutman, M., Zupaneč, B., Lesar Kikelj, M., Kramar, S., 2016. Wall paintings from the roman emona (Ljubljana, Slovenia): Characterization of mortar layers and pigments. *Archaeometry* 58 (2), 297–314. <https://doi.org/10.1111/arc.12167>.
- Izzo, F., Arizzi, A., Cappelletti, P., Cultrone, G., de Bonis, A., Germinario, C., Graziano, S. F., Grifa, C., Guarino, V., Mercurio, M., Morra, V., Langella, A., 2016. The art of building in the Roman period (89 B.C. - 79 A.D.): Mortars, plasters and mosaic floors from ancient Stabiae (Naples, Italy). *Constr. Build. Mater.* 117, 129–143. <https://doi.org/10.1016/j.conbuildmat.2016.04.101>.
- Jabaloy Sánchez, A., Martín-Algarra, A., Padrón-Navarta, J.A., Martín-Martín, M., Gómez-Pugnaire, M.T., López Sánchez-Vizcaíno, V., Garrido, C.J., 2019. Lithological successions of the internal zones and flysch trough units of the Betic Chain. In: *The Geology of Iberia: A Geodynamic Approach*, Vol. 3. Springer, Cham, pp. 377–432. https://doi.org/10.1007/978-3-030-11295-0_8.
- Karim, M.E., Alam, M.J., Hoque, S., 2017. Effect of salinity of water in lime-fly ash treated sand. *Int. J. Geo-Eng.* 8, 15.
- Lancaster, L.C., 2021. Mortars and plasters—How mortars were made. *The Literary Sources. Archaeological and Anthropological Sciences* 13 (11), 1–20. <https://doi.org/10.1007/s12520-021-01395-0>.
- Lewit, T., 2008. Rural life in late-antique Hispania. *Journal of Roman Archaeology* 21, 725–727. <https://doi.org/10.1017/S1047759400005183>.
- López-Martínez, T., López Cruz, O., García Bueno, A., Calero- Castillo, A.I., Medina Flórez, V.J., 2016. Las pinturas murales de Castulo. Primeras aportaciones a la caracterización de materiales y técnicas de ejecución. *Lucentum* 35, 155–170. <https://doi.org/10.14198/LVCENTVM2016.35.08>.
- Montana, G., Randazzo, L., Vassallo, S., Udine, F., 2018. The mosaic of the frigidarium of “Villa Bonanno” in Palermo: mineralogical and petrographic analyses for in situ conservation and restoration interventions. *Mediterr. Archaeol. Archaeom.* 18 (5), 95–107.
- Lapuente, P., Martínez, M.P., Turi, B., Blanc, P., 2022. Characterization of dolomitic marbles from the Malaga province (Spain) in interdisciplinary studies on ancient Stone, pp. 152–162.
- Moreno, M.A., De Luxan, M.P., Dorrego, F., 1997. The conservation and scientific investigation of the wall paintings in the Roman thermes, Campo Valdes, Gijón, Spain. In: Bearat, H., Fuchs, M., Maggetti, M., Paunier, D. (Eds.), *Roman Wall Painting: Materials, Techniques, Analyses and Conservation*, *Proceedings of the International Workshop*, Fribourg 7–9 March 1996., Institute of Mineralogy and Petrology, Fribourg University, pp. 297–306.
- Moreno Prieto, C., Vila Oblitas, M., 2022. Memoria preliminar Actividad arqueológica urgente: Sondeos y estudio para la conservación y consolidación de los restos aparecidos en Duna Playa Linda Vista, San Pedro Alcántara. T.M. Marbella, Informe administrativo.
- Ontiveros-Ortega, E., Fortes, J.B., Azuaga, M.L.L., 2019. Mineralogical petrographic and geochemical characterization of marmora from the Roman quarries of Cabra (Córdoba) and Antequera (Málaga), external sector areas of the betic Chain. Spain. *Journal of Archaeological Science: Reports* 27, 101956. <https://doi.org/10.1016/j.jasrep.2019.101956>.
- Pagano, S., Germinario, C., Alberghina, M.F., Covolan, M., Mercurio, M., Musmeci, D., Piovesan, R., Santoriello, A., Schiavone, S., Grifa, C., 2022. Multilayer technology of decorated plasters from the domus of marcus vipsanus primigenius at abellinum (Campania Region, Southern Italy): An analytical approach. *Minerals* 12 (12), 1487. <https://doi.org/10.3390/min12121487>.
- Pérez de Barradas, J.A., 1930. Excavaciones en la colonia de San Pedro de Alcántara, Málaga. Junta Superior del Tesoro Artístico. In: *Sección de Excavaciones y Antigüedades*, n°2., Tipografía de archivos, Madrid, España, pp. 3–14.
- Pérez de Barradas, J., 1932. La Basílica Paleocristiana de Vega del Mar (San Pedro de Alcántara, Málaga). *Archivo Español de Arte y Arqueología* 8 (22), 53.
- Pérez de Barradas, J.A., 1934. Excavaciones en la Necrópolis visigoda de Vega del Mar. San Pedro de Alcántara, Málaga. Junta Superior del Tesoro Artístico. In: *Sección de Excavaciones*, n°3., Tipografía de archivos, Madrid, España, pp. 5–47.
- Piovesan, R., Siddall, R., Mazzoli, C., Nodari, L., 2011. The Temple of Venus (Pompeii): A study of the pigments and painting techniques. *J. Archaeol. Sci.* 38 (10), 2633–2643. <https://doi.org/10.1016/j.jas.2011.05.021> &
- Pérez-Rodríguez, J.L., de Haro, M., del, C.J., Siguenza, B., Martínez-Blanes, J.M., 2015. Green pigments of Roman mural paintings from Seville Alcazar. *Appl. Clay Sci.* 116–117, 211–219. <https://doi.org/10.1016/j.clay.2015.03.016>.
- Piovesan, R., Mazzoli, C., Maritan, L., Cornale, P., 2012. Fresco and lime-paint: An experimental study and objective criteria for distinguishing between these painting techniques. *Archaeometry* 54 (4), 723–736. <https://doi.org/10.1111/j.1475-4754.2011.00647.x>.
- Puerto Fernández, J.L., Fernández Martín, A., Melero García, F., Vila Oblitas, M., 2017. Prospección geofísica de georradar en la Basílica paleocristiana Vega del Mar (Marbella). *Anuario Arqueológico de Andalucía*.
- Puertas Tricas, Posac Mon, C., 1989. La basílica paleocristiana de Vega del Mar (San Pedro de Alcántara, Marbella). In: *Colección de Monografías*, n°2., Servicio de Publicaciones, Diputación Provincial de Málaga.
- Requena Cueto, M., 2021. Actividad arqueológica urgente de cubrición de estructuras en el entorno de la Basílica Paleocristiana de Vega de Mar, San Pedro Alcántara. Memoria administrativa, Junta de Andalucía.
- Rodríguez-Navarro, C., Ilic, T., Ruiz-Agudo, E., 2023. Carbonation mechanisms and kinetics of lime-based binders: An overview. *Cem. Concr. Res.* 173, 107301.
- Salvadori, M., Sbrolli, C., 2021. Wall paintings through the ages: The roman period—Republic and early Empire. *Archaeol. Anthropol. Sci.* 13 (11), 1–30. <https://doi.org/10.1007/s12520-021-01411-3>.
- Siddall, R., 2018. Mineral pigments in archaeology: Their analysis and the range of available materials. *Minerals* 8 (5), 201. <https://doi.org/10.3390/min8050201>.
- Torres-Roldán, R.L., García-Casco, A., García-Sánchez, P.A., Torres-Roldán, R.L., García-Casco, A., García-Sánchez, P., 2000. CSpace: An integrated workplace for the graphical and algebraic analysis of phase assemblages on 32-bit wintel platforms. *Comput. Geosci.* 26, 779–793. [https://doi.org/10.1016/S0098-3004\(00\)00006-6](https://doi.org/10.1016/S0098-3004(00)00006-6).
- Tsantini, E., Minami, T., Takahashi, K., Ontiveros, M.A.C., 2018. Analysis of sulphur isotopes to identify the origin of cinnabar in the Roman wall paintings from Badalona (Spain). *J. Archaeol. Sci. Rep.* 18, 300–307. <https://doi.org/10.1016/j.jasrep.2018.01.032>.
- Tuñón, J., Sánchez, A., Parras, D.J., Amate, P., Montejo, M., Ceprián, B., 2020. The colours of Rome in the walls of Cástulo (Linares, Spain). *Sci. Rep.* 10 (1), 1–15. <https://doi.org/10.1038/s41598-020-69334-y>.
- IGME (Instituto Geológico y Minero de España), LNEG (Laboratorio Nacional de Energía y Geología de Portugal), 2015. Editors: L.R. Rodríguez Fernández J.T. Oliveira F. López Olmedo R.P. Dias T. Medialdea Cela P. Terrinha Authors: L.R. Rodríguez Fernández F. López Olmedo J.T. Oliveira T. Medialdea Cela P. Terrinha J. Matas González A. Martín-Serrano García L.M. Martín Parra F. Rubio Pascual C. Marín Lechado M.y. Montes Santiago F. Nozal Martín *Mapa Geológico de España y Portugal* (Scale 1:1.000.0000).
- Fuchs, M., Bearat, H., 1997. Analyses physicochimiques et peintures murales romaines a Avenches, Böisingen, Dietikon et Vallon. In: Bearat, H., Fuchs, M., Maggetti, M., Paunier, D. (Eds.), *Roman Wall Painting: Materials, Techniques, Analyses and Conservation. Proceedings of the International Workshop*, Fribourg 7–9 March 1996. Institute of Mineralogy and Petrology, Fribourg University, pp. 181–192.
- Varian, A., Bearat, H., 1997. Pittori romani al lavoro. Materiali, strumenti, tecniche: evidenze archeologiche e dati analitici di un recente scavo pompeiano lungo via dell'Abbondanza (reg. IX ins. 12). In: Bearat, H., Fuchs, M., Maggetti, M., Paunier, D. (Eds.), *Roman Wall Painting: Materials, Techniques, Analyses and Conservation. Proceedings of the International Workshop*, Fribourg 7–9 March 1996., Institute of Mineralogy and Petrology, Fribourg University, pp. 199–214.
- Velasco, J.S., 2018. *The Christianization of Western Baetica: Architecture, Power, and Religion in a Late Antique Landscape*. Amsterdam University Press B.V, Amsterdam.
- Villar, S.E.J., Edwards, H.G.M., 2005. An extensive colour palette in Roman villas in Burgos, Northern Spain: A Raman spectroscopic analysis. *Anal. Bioanal. Chem.* 382 (2), 283–289. <https://doi.org/10.1007/s00216-004-2876-7>.
- Villaseca Díaz, F. y Garrido Luque, A., 1991. Actuación arqueológica de urgencia en la Duna de San Pedro de Alcántara, Marbella, A.A.A. 1991, Tomo III, Málaga, pp. 389–390.
- Villasenor, I., Price, C.A., 2008. Technology and decay of magnesian lime plasters: the sculptures of the furnace crypt of Palenque, Mexico. *J. Archaeol. Sci.* 35, 1030–1039.
- Wyszecki, G., Stiles, W.S., 1982. *Colour science. Concepts and methods, quantitative data and formulae*, 2nd ed. J. Wiley & Sons, New York.